2011

Temporal and Spatial Variation of Fine Sediment Infiltration in a Gravel-Bed River

Elena Gronli Evans
The University of Montana

Temporal and Spatial Variation of Fine Sediment Infiltration in a Gravel-Bed River

By

Elena Gronli Evans

Bachelor of Arts, Macalester College, St. Paul, Minnesota, 2006

Thesis

Presented in partial fulfillment of the requirements of the degree of

Master of Science

in Geosciences

The University of Montana

Missoula, Montana

Fall 2011

Approved by:

Dr. Perry Brown, Associate Provost for Graduate Education

Graduate School

Dr. Andrew Wilcox, Chair

Department of Geosciences

Dr. Johnnie Moore

Department of Geosciences

Dr. Scott Woods

Department of Ecosystem and Conservation Science

Evans, Elena G., M. S., Spring 2011 Geosciences

Temporal and Spatial Variation of Fine Sediment Infiltration in a Gravel-Bed River

Committee Chair: Dr. Andrew Wilcox

Pulses of fine sediment in gravel-bedded rivers can cause extensive fine sediment infiltration (FSI), potentially altering river morphodynamics and aquatic ecosystems. FSI occurs when sand and silt are deposited into void spaces between larger grains at the riverbed. Flume and theoretical modeling provide a background for a conceptual model of FSI in natural systems. In this model, FSI will occur to a limited depth as a function of the relative grain size of bed sediment to infiltrating sediment. At a larger scale, fine sediment supply, feed rate and local flow dynamics also dictate the extent of FSI. In 2008, the Milltown Dam near Missoula, MT was removed as part of a Superfund remediation action and released contaminated sediment downstream. I used bulk sampling, freeze cores, infiltration bags and a suspended sediment water bottle to collect samples for metal analysis and comparison with USGS data. The analysis of these metal concentrations indicates that the sediment associated with the dam removal, identified by the highest metal concentrations, is not found in the bed of the field site 14 km downstream. Pore space through the reach was either full when the dam removal sediment pulse fluxed through the field site or the substrate has been reworked. Fine sediment fractions from bulk samples are lowest in riffles, have intermediate values in main channel and complex flow areas and the highest fractions in backwater areas. At depth and across depositional settings, fine sediment has multi-year residence times. My work suggests that because the timing and spatial variability of substrate reworking strongly influence fine sediment content in river beds, understanding of such factors is essential to remediation efforts concerned with fine sediment infiltration.

Acknowledgements:

I could not have done this alone and thank friends, family and colleagues for their support. I would like to thank my mentor and advisor, Andrew Wilcox, for his time and guidance. His valuable critiques and direction were critical to this work. Committee member, Johnnie Moore provided important direction and feedback that shaped this thesis. Scott Woods provided feedback and perspective. Field work would not have been possible without the help of field assistants Kelley Garrison, Rob Livesay, Matt Gilbert , Ryan Carter, Annika Stoner, Ashley Williams, Pete Ferranti, and Doug Brinkerhoff. I would also like to express gratitude to these kind people who volunteered their time in the name of science Ivan Orsic, Adrienne Keller, Megan Keville, Blase Reardon, Erin Grinde, Walker Hoen, Zach Seligman, Molly Staats, Megan Rosenblatt and Tim Wheeler. Additionally, I would also like to thank Loreene Skeel, Christine Foster, Wendy Wollett, Matt Young, Aaron Deskins and the UM Geomorphology Lab. Freeze coring would not have been possible without the generous donation of equipment from Aleksandra Wyzdga. Advice from Heiko Langner and Leonard Sklar also helped direct fieldwork. This research was made possible through funding/grants provided by the National Science Foundation (NSF EAR-0922296, NSF EPS-0701906) the Montana Water Center, the Rocky Mountain Section of the Society of Economic Paleontologists and Mineralogists, and the Geologic Society of America.

Table of Contents

Figures

Tables

1. Introduction

1.1 Fine Sediment Infiltration

Fine-grained sediment infiltration can degrade habitat for macroinvertebrates, salmonids, and other aquatic organisms (Richards and Bacon, 1994) by reducing intragravel flow, decreasing oxygen available to salmonid embryos and inhibiting oxygen exchange across embryo membranes (Greig et al., 2005; Suttle et al., 2004). In gravel-bed rivers there is usually a wide range of grain sizes of sediment in transport. Larger grains on the bed of the river can create interstitial space (pore space) where smaller-grained sediment can deposit. Depending upon the mixture of sediment, there are different porosities or amounts of pore space (Standish and Borger, 1979). Fine sediment infiltration (FSI) occurs when fine-grained sediment (< 2mm) is deposited into the pore space of a gravel matrix. Kleinhans and Van Rijn (2002) call this process unimpeded static percolation.

In one of the first FSI experiments, Einstein (1968) used a recirculating flume to feed fine quartz (0.0035 to 0.03 mm) into clean gravel and found fine sediment first settles at the bottom of the flume and then fills the pore space above. Beschta and Jackson (1979) used 0.2-0.5mm sand in a gravel bed composed of 4.5-50 mm gravel. In this study, fine sediment only infiltrated to a depth approximately twice the diameter of the largest bed material. Diplas and Parker (1985) conducted a similar experiment holding the bed matrix size constant and varying the fine sediment size. Samples of bed material following runs with 0.2-mm sand feed had almost double the sand than the runs using 0.5-mm sand. Gibson et al. (2009), investigating the control of grain

size on the vertical distribution of infiltrated fine sediment, describe grain size distributions in terms of separate gravel and fine sediment components, where $D_{\text{percent finer than}}$ describes the size distribution for gravel and $d_{\text{percent finer than}}$ describes the fine sediment. They found that the ratio D_{15}/d_{85} accurately characterizes the trapping efficiency of gravel. These sizes were chosen because at this grain size ratio the larger fine grains can get caught in the smaller gravel and block further infiltration from occurring. Gibson's study found that when grain size ratios (D_x/d_x) were 10 to 6, samples created a seal, cutting off most deeper infiltration. When ratios were 15 to 4, FSI occurred to depths similar to the Einstein (1968) experiment. Characterizing the average grain size and the distribution of grain sizes can provide insight into the porosity of the substrate (Sulaiman et al., 2007). The larger grains are, the more space there is for smaller grains, but if there is a wide range of grain sizes present they can fit into the pore space, leaving less room for FSI (Fig. 1).

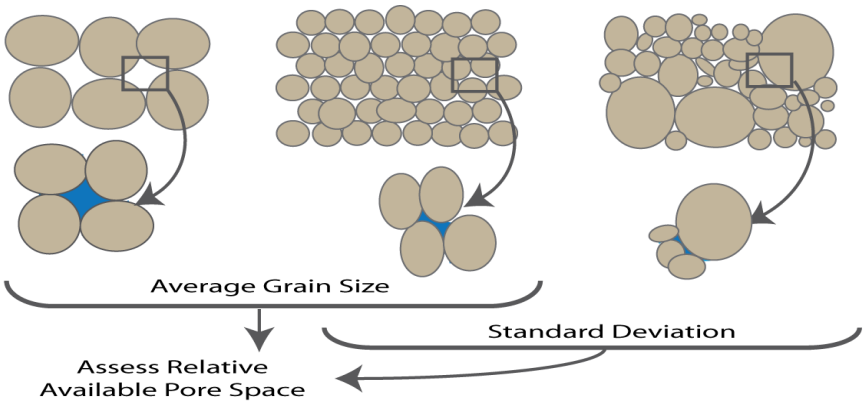

Figure 1. Conceptual diagram of the role average grain size and standard deviation play in determining available pore space. If grain size distributions are similar, the distribution with the larger the average grain size will have more pore space.

Together these studies indicate that the relative size of the gravel and the infiltrating sediment dictate the pore size and the extent of infiltration.

To quantify the relative effects of grain size on FSI, Cui et al. (2008) analyzed fine sediment content from flume studies by Wooster et al. (2008). They used governing equations derived from mass conservation as well as the assumption that FSI and deposition at depth is constant or increases with greater fine sediment fractions. This work builds on a study by Sakthivadivel and Einstein (1970) but corrects the assumption in the earlier model that intragravel flow remains constant. The Cui/Wooster model found that FSI is "negatively correlated to the standard deviation of particle diameters within the gravel deposit" and decreases with depth.

Leonardson (2010) refined Wooster's model by incorporating different equations for the fine structures resulting from and affecting FSI. Larger infiltrating grains can get lodged near the surface of the bed, blocking available interstitial space below and impeding further infiltration. This structure has been called a bridge in some studies but for this study is a seal. FSI is also affected by the piling of sand on top of gravel grains where particle packing largely determines accommodation of fines. Leonardson created a new model with a variable trapping coefficient to better predict fine sediment fraction when grain size is $7 < (D_{15}/d_{85}) < 14$. This incorporates a particle-packing relationship adopted from Ridgway and Tarbuck (1968) and develops an infiltration model that calculates subsurface flow in the upper pore spaces. Therefore, the highest fine sediment fraction due to infiltration in a clean bed is determined by the relative grain sizes of matrix sediments compared to the fine-grained sediments and is limited by depth.

Relative grain sizes dictate FSI and these are controlled by sediment in the substrate and sediment supply. Diplas and Parker (1985) found that fine sediment saturation, infiltration of all pore space, eventually occurs if fine sediment is available in the water column, regardless of

concentration. Wooster et al. (2008) conducted three flume runs with each feed rate of fine sediment ten times greater than the previous run. The highest sand feed rate produced less sand infiltration than the other two runs, which were comparable. The sand input also created different widths of active sand transport that coincided with the location of infiltration. Portions of the flume in contact with the active transport belt became saturated with fines first. Flume studies find fine sediment will infiltrate if present in the water column to a limited depth dependent upon feed rate (Wooster et al., 2008). These flume studies find fine sediment infiltration will occur within the constraints of flume studies but cautioned that sediment routing may be particularly important in complex natural settings.

The transport of sediment can alter the order in which different sized grains arrive to open pore space. Gibson et al. (2009) explained the fining of interstitial sand as a function overlapping processes: granular sorting, bedload sorting and hydraulic sorting. Similar to the theoretical models, granular sorting is a function of finer grains depositing deeper in the substrate. Bedload sorting separates grain size in the wake of the leading bed form as smaller grains saltate further. Hydraulic sorting occurs because smaller grains can be transported as suspended sediment and travel further downstream, filling interstitial space downstream before bedload arrives. This experiment also found higher shear stress led to greater transport of larger grains allowing seals to form more quickly, sealing off underlying pore space from FSI. Shear stress can also alter the availability of pore space. Allan and Frostick (1999) found that dilation of matrix sediment occurs at shear stresses just before entrainment of framework material. Dilation allows greater and deeper infiltration of sediment. Winnowing of fine sediment from upper layers of the

substrate can also create pore space. Sorting mechanisms determine FSI by altering the grain size distributions of fine sediment in transport and available pore space.

Field studies are necessary to confirm flume studies and conceptual models within the context of natural systems. Frostick et al. (1984) conducted the first field study of FSI, hypothesizing that subsurface to surface grain size distributions were important. However, this can also be described as a function of particle diameter variation in the context of the Cui/Wooster/Leonardson equations. Frostick et al. (1984) further found that FSI was high in areas of high velocity whereas Carling and McCahon (1987a) found slack waters had high rates of FSI. Sear (1993) investigated the relationship between FSI and shear stress, finding a negative correlation for suspended sediments and no relationship for bedload. Lisle (1989) conducted a comprehensive field study of FSI in three rivers using infiltration cans and freeze cores in conjunction with suspended and bedload transport measurements. The study found intragravel flow contributed on average 6-8% of infiltrated sediment and fewer fines were deposited in riffle crests, perhaps due to elevated winnowing as a result of increased turbulence. By comparing sediment deposited from suspension and from bedload, Lisle (1989) found sediment settling from suspension does not account for most of the infiltrated sediment. Rather, grain sizes are usually smaller and can deposit deeper than the bedload-transported larger sediment. The finest sediment transported as bedload was the most common infiltrated grain size. Mean bankfull shear stress was calculated with bedload particles and exceeded threshold shear stress but could not account for the variability in infiltration. The field studies described above support flume and theoretical models of FSI but additional studies of natural systems are needed to account for the large variability of FSI and feedbacks between infiltration and local flow dynamics.

The conceptual model of FSI that I have developed, based on synthesis of the literature, is that the depth and volume of infiltration is dependent upon the relative size of the gravel substrate to the infiltrating fine sediment, fine sediment supply and local hydraulics (Fig. 2).

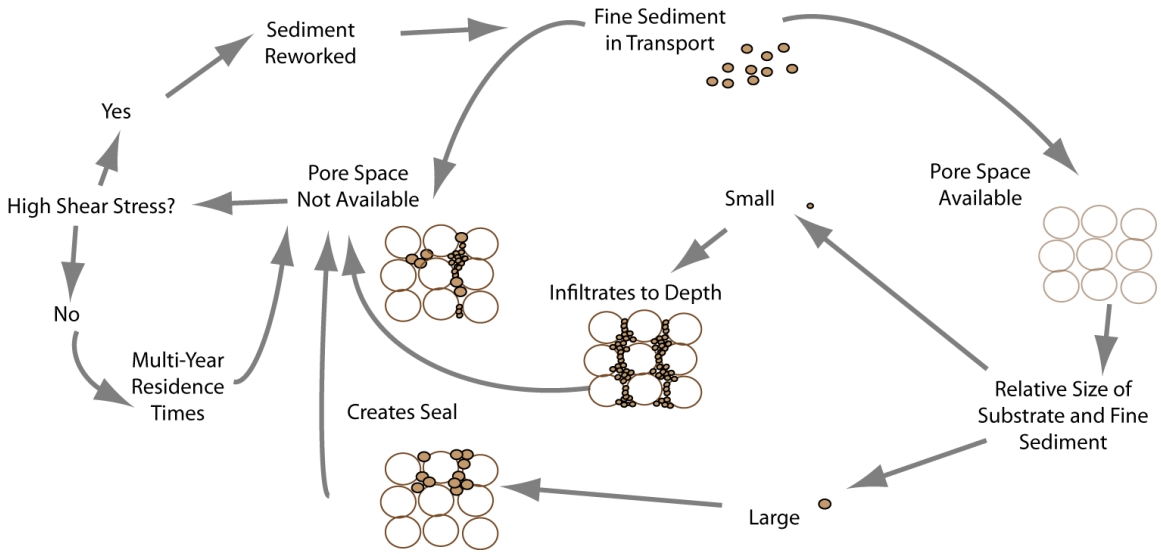

Figure 2: Conceptual model of fine sediment infiltration. Fine sediment must be in transport and can only infiltrate if pore space is available. The structure of infiltration depends upon the relative size of substrate and fine sediment. High shear stress can cause reworking of the bed.

1.2 Sediment Transport

Channel features alter sediment routing and deposition through the introduction of roughness elements, formation of secondary flow and partitioning of flow. In-channel features cause flow deviation from streamlines. These small perturbations in the flow can grow into vortices and turbulent eddies. Through the winnowing of fines by turbulence in eddies, larger particles are preferentially deposited as fine sediment is transported away (Clifford et al., 1993). Turbulent eddies can propagate downstream, dissipating primary flow and increasing the effect of preferential deposition. This effect is called eddy viscosity (Dingman, 2009) and depends upon

the mixing length and velocity gradient (Prandtl, 1925). Roughness elements cause secondary flow by creating turbulence.

Curvature of streamlines by meander bends or islands also introduce secondary flow. In straight channels, velocity gradients decrease when encountering roughness elements, with the fastest flow at the surface in the middle of the channel. Islands and bars cause streamlines to curve, which changes velocity gradients. Curvature causes centrifugal force to carry the faster surface velocity closer to the bend. The slower moving surface velocities on the inside of the bend results in helicoidal circulation and superelevation or tilting of water elevation (Dietrich et al., 1979). This circulation contributes to erosion on the outside of the bend and deposition on the inside curve. Pressure gradients induced by superelevation cause lower shear stress on the inside of the curve and deposition of fine sediment (Bridge and Lunt, 2006). Fine sediment has a larger surface area to mass ratio and will not be deflected down slope as directly as coarser grains (Paola, 1989). Streamline curvature causes preferential deposition of fine sediment on the inside of curves with cross channel slope dictating the deposition of larger grains. Patches of differing grain size may cause further preferential deposition of like grain sizes (Bluck, 1987) and could result in the formation of stable bedforms (Kleinhans, 2010).

Islands are similar to meander bends because flow diverges around either side of the island creating curved streamlines on both sides. Flow shoals onto the upstream end of the island, depositing larger grain sizes that maintain momentum and avoid deflection into the diverging flow paths. Secondary circulation cells are created on both sides of the island. These flow structures cause grain size partitioning on both sides of the island. Areas of high velocity on

either side of the channel accelerate and converge at the downstream boundary. The transverse slope caused by growth of the bar allows particles on these slopes to be more readily entrained (Parker, et al., 2003; Vollmer and Kleinhans, 2007).

In multi-thread channels, topographic steering of flow and sediment is further dictated by channel confluence and bifurcation. The hydraulic and sediment routing downstream from a confluence depends upon the channel planform geometry and relative velocity and discharge of channels (Ashmore and Gardner, 2008). The geometry of the channels dictates the angle at which flows merge and the resulting turbulence and shear that are created. Scour pools can develop at the convergence if the angle between the channels is greater than 15 degrees, the channels are sufficiently deep and sediment delivery is low (Mosley, 1976). If one channel is smaller than the other, the larger channel could prograde into the scour pool (Ashmore, 1982). The river downstream of the confluence axis will shift to be aligned more closely with the larger channel.

Even in straight reaches, topographic highs and lows in the form of riffles and pools can evolve. Riffles are generally shallower, have a higher velocity, more turbulence and coarser grain sizes. Pools are deeper, have lower velocities and finer grain sizes relative to riffles. These forms could be caused by a meandering thalweg that causes convergent and divergent flow patterns (Keller, 1972). Channel constrictions at the pool head cause recirculating eddies (Thompson et al., 1996) Sediment routing through pools is largely driven by these eddies as sediment is steered away from the deepest part of the pools. Portions of multi-thread channels may contain pool-riffle units (Ashmore and Gardner, 2008)

Multi-thread channels often have many in channel features that can alter local hydraulics and create secondary flow. The partitioning of flow and sediment routing results in preferential deposition of grain sizes (Kleinhans, 2010). Sediment entrainment and settling rates are largely dictated by grain size and velocity. Fine sediment is most sensitive to flow separation and may result in higher rates of FSI. Gravel bedded rivers often entrain greater sediment size distributions, and flow separation may dictate areas of increased FSI.

Bed morphology and sediment transport dynamics can also be altered by fine-grained sediment infiltration (Lisle and Hilton, 1999; Dietrich et al., 1989). FSI can smooth the bed, which could decrease bed mobility by limiting protrusion and reducing the friction angle of particles (Kirchner et al., 1990) or alternatively increase mobility by increasing near-bed velocities (Ikeda, 1984). Downstream fining and relative sizes dictate which sediment sizes are pore-filling versus bed structure load (Frings et al., 2008).

Changes in bed mobility induced by infiltration could alter the residence time of the substrate; when gravel is more difficult to entrain, the bed is less likely to be reworked and residence time of substrate increases (Venditti et al., 2010). Therefore, accommodation of fines is also related to the rate of supply, with substrate mobility further dictating residence time of infiltrated fines.

Flume and field studies provide a conceptual model of FSI but do not provide sufficient data at appropriate spatial and temporal scales in natural systems to guide restoration and mitigation efforts. The removal of the Milltown Dam in western Montana in 2008 provided an opportunity

for a large-scale field experiment. The removal resulted in a fine-grained, contaminated sediment pulse, enabling investigation of FSI in a complex, natural stream network.

1.3 Metal Contaminants in Fluvial Systems

Fingerprinting of sediments can provide the origin of sediments and in some instances timing, providing further control in field studies. Different properties have been used to identify origin or source. The effectiveness of these properties is enhanced with the use of mixing models (Shankar et al., 1994; Walden et al., 1997) and analysis of variance (Walling and Woodward, 1995). The fingerprinting of sediment has been used to identify surface versus subsurface sources (Gruszowski et al., 2003). This technique can also be used to associate surface soils with different land use practices (Wallbrink et al., 2003; Slattery et al., 2002). On a catchment scale, fingerprinting has been used to determine tributary of origin (Collins et al., 1996; 1997). Ashley et al. (2006) assessed an array of contaminants prior to and following a dam removal. They found the removal of the small dam did not result in significant change in the distribution of contaminants but noted this result is site specific. Characteristics of fine sediment have been used to identify sources of origin in order to proactively reduce the siltation of gravel beds (Bluck, 1987; Walling et al., 2003).

Fluvial systems have long been impacted by mining operations (Salomons, 1995). Direct runoff from mine sites and reworking of tailings piles introduce metal-contaminated sediment to fluvial systems. Geomorphic processes then distribute metal-contaminated sediment downstream, depositing these sediments in the bed, on the banks and on the floodplains as a function of sediment size, mixing processes and hydraulic conditions (Horowitz, 1984). Fine-grained

sediments have a greater surface area to volume ratio and usually have higher metal concentrations, although metals can accumulate on larger grain surfaces (Foster and Charlesworth, 1996).

Sediment transport processes in river systems have a large role in the dispersal, storage and remobilization of metal contaminants. More than 90% of metal contaminants in river systems are transported as a function of geomorphic processes in particulate-associated form (Martin and Meybeck, 1979). If most metal contaminants are transported as particulates, the temporal and spatial dynamics of river systems dictate metal contaminant dispersion.

1.4 Clark Fork River and Milltown Dam History

Mining began in Butte in 1864 and smelters were built in 1919. Since then, mining and smelting operations have introduced metal-contaminated sediment into the Clark Fork River (Moore and Luoma, 1990). The Milltown dam was first built in 1907 below the confluence of the Blackfoot River (BFR) and Clark Fork Rivers (CFR) with an upstream drainage area of 15,700 km^2. In 1908, a 300-500 year flood washed down the Clark Fork and deposited millions of cubic meters of sediment behind the new dam. The sediment included mine tailings from upstream. The inclusion of these metal contaminated sediments created a metal signature unique to the Milltown reservoir. Key elements within this metal signature are arsenic, copper, lead and zinc concentrations within the reservoir which are all above background levels (Johns and Moore, 1985; Andrews, 1987; Moore et al., 1988). Reservoir sediments are primarily fine-grained coarsening upstream to cobble in the Blackfoot arm (BFA) (Envirocon, 2004) and to fine gravel in the Clark Fork arm (CFA) (Titan, 1995). Elevated levels of trace metals in the water and

sediment in the CFA and upstream led to its designation as an extended National Priority Superfund Site in 1983 (U.S. Environmental Protection Agency, 2004). Ice jams in 1996 released contaminated sediment downstream and caused further concern about the structural integrity of the dam (Moore and Landrigan, 1999). In 2004, the U.S. Environmental Protection Agency determined the removal of the Milltown Dam would be one of the remediation activities.

In 2006, the reservoir was drawn down 3.7 m and construction of a bypass channel through the lower half of the CFA began. The most contaminated sediment in the reservoir was mechanically removed and shipped away by rail. While contaminated sediment was being removed, the Clark Fork River was routed through a bypass channel. Erosion of the BFA and upper CFA was still anticipated with most of the sediment coming from the uncontaminated BFA.

On March 28, 2008, the cofferdam was breached. The BFA incised quickly, releasing uncontaminated sediment downstream. The response of the CFA lagged due to the hardening of the bypass channel that anchored the Clark Fork River in place. Upstream of the hardened channel, the upper reservoir channel widened during the 2008 peak flows (Wilcox et al., 2009).

USGS conducted intensive suspended sediment and water sampling in an effort to monitor the effects of remediation actions (Lambing et al., 2009). Sampling was conducted upstream of the reservoir at the USGS gage Clark Fork at Turah Bridge, near Bonner (12334550) in the CFA and in the BFA at the USGS gage Blackfoot River near Bonner (12340000). Subtracting the inputs to the reservoir from the discharge found at the downstream gage, the USGS gage Clark Fork above Missoula (12340500), allowed calculation of estimated daily cumulative loads of suspended

sediments and arsenic (As), cadmium (Cd), copper (Cu), iron (Fe), lead (Pb), and zinc (Zn) (Lambing and Sando, 2009). In addition to these long-term gages, a supplemental gage, Clark Fork Bypass near Bonner, Mont. (12334570), was monitored during 2008. The post breach suspended sediment load was 22 times greater than pre-breach sediment loads; 142 metric tons of Cu, 20.4 metric tons of Pb and 222 metric tons of zinc eroded from the reservoir in 2008. These net losses were 2 to 4 times greater than the metal losses in 2007 when the reservoir was drawn down (Lambing et al., 2009).

Field based topographic studies of the BFA found channel adjustment and incision occurred quickly. Peak erosion in the BFA occurred shortly after the peak in the hydrograph releasing 150,000 m^3 in the first year following the dam removal (Epstein, 2009). Initial bedload samples out of the reservoir were primarily (>90%) sand and smaller. Fine-grained sediment dominated bedload transport until halfway through the rising limb of 2009 hydrograph (Johnsen, 2011). There are peaks in sediment load that correspond with each peak in discharge but the peak in metal load associated with the dam removal in 2008 has a uniquely higher flux of both sediment and metal load downstream (Fig. 3).

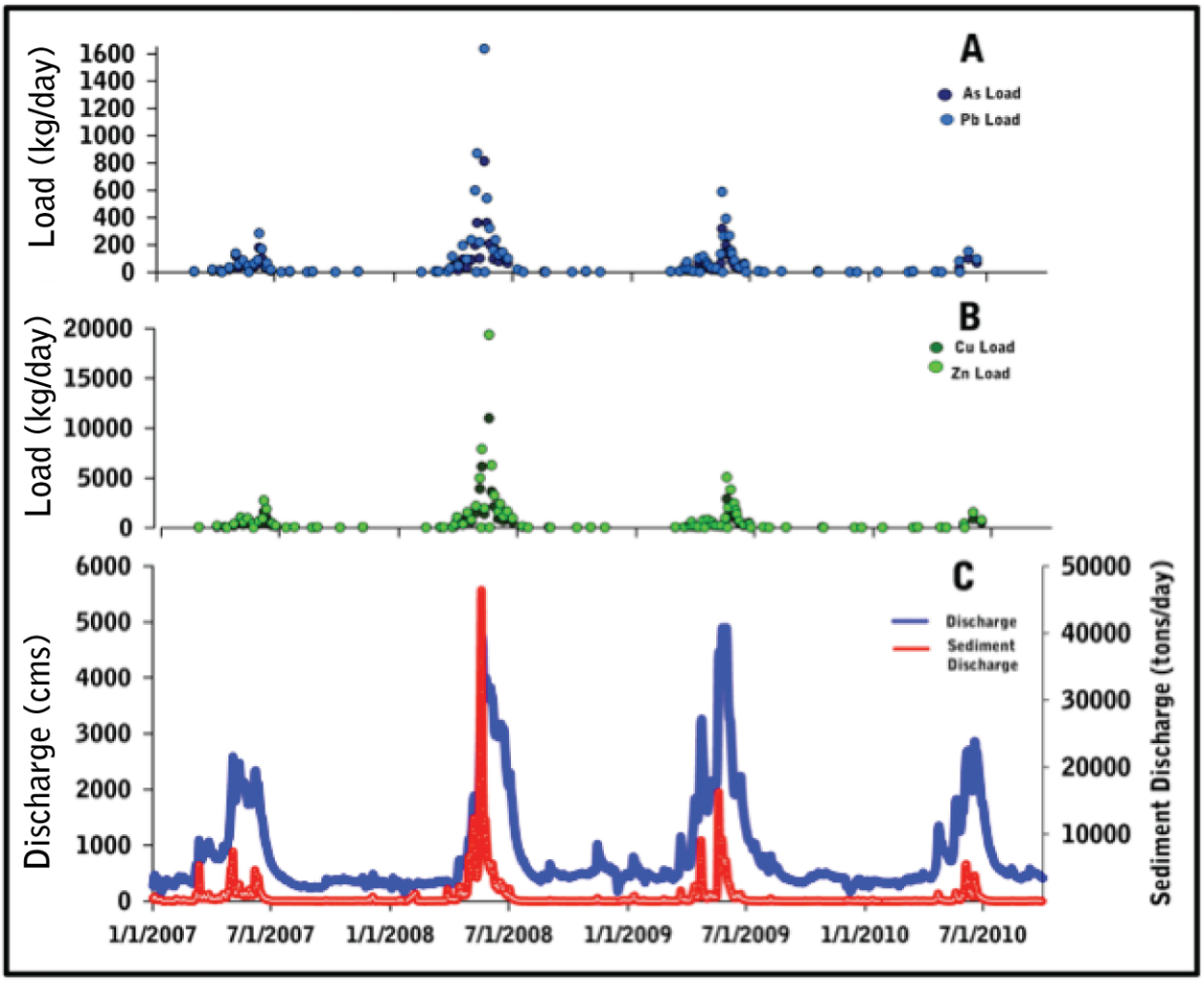

Figure 3.The Clark Fork Above Missoula MT Gage 12340500 arsenic and lead load (A), copper and zinc load (B), sediment load and discharge (C) for the four years following the initial drawdown of Milltown reservoir in preparation for the Milltown dam removal. Suspended sediment loads indicate a distinct sediment pulse in 2008 with suspended sediment loads almost an order of magnitude lower in 2010.

1.5 Field site

The field area for this study is a 1 km reach of the Clark Fork River, MT, referred to hereafter as the Tower Street reach, located 16 km downstream of the former site of the Milltown Dam in an anastomosing, multi-thread reach of the river (Fig. 4). In the 14 km downstream of the Milltown dam site, the Clark Fork River has a high transport capacity and is single thread with a longitudinal slope of 0.0015. Upstream of the Tower Street reach, the channel becomes multi-

thread, which could impact sediment transport dynamics. Within the Tower Street reach the slope is 0.0021, and there are three distinct channels and two islands. Two channels converge asymmetrically. Just upstream of the convergence, a portion of the main channel diverges through a riffle. In the secondary channel, the flow bifurcates around an island just upstream of the confluence creating riffles on either side of the island and a backwater pool behind the island. Flow from the main channel and the secondary channels converge downstream from the two islands just upstream of the larger channel convergence, creating a complex flow environment.

Following the dam removal, significant deposition of sediment was observed in the Tower Street reach in side channels, flood plains, bars and banks. Preliminary metal analyses suggest sediment from the CFA of the reservoir deposited on the banks and floodplains of the field site on top of an inferred pre-dam removal surface. The subaerial deposit above the CFA sediment is relatively uncontaminated and may be BFA sediment (Orsic, In Progress).

Figure 4. Location map showing field site within the multi-thread Tower Street Reach and the site of the Milltown Dam. Right hand inset map shows location of larger map in Montana. Left hand inset map is a close up of the fieldsite, which is shown in detail in Figure 5.

Drawing upon the conceptual model of infiltration described above and using contaminated sediment to fingerprint sediment timing and origin of infiltration, this study investigates the following hypotheses:

1) Infiltrated sediment in the bed of the study reach originated from the sediment pulse produced by the removal of the Milltown dam.

2) FSI varies by depositional setting and is highest in recirculation zones associated with bifurcations and confluences in multi-thread channels.

3) Once fines have infiltrated, fine sediment in the substrate has multi-year residence times.

2. Methods

Methods include bulk sampling, freeze cores, infiltration bags, suspended sediment water bottles, analysis of USGS metal concentration data and metal analysis. Field methods were subjectively distributed across different depositional environments (Fig. 5). This study focuses on areas of lower transport capacity such as side channels and back eddies where there is more sediment deposition. Grouping samples by qualitative assessments of depositional setting allows for generalization about FSI by depositional setting. Main channel samples are located in lower transport capacity areas at base flow but high transport areas during peak flow. Secondary channel samples are subject to different flow and sediment routing and located in low transport areas of the secondary channel. Areas of flow divergence and convergence are grouped under complex flow because these areas change over the course of the hydrograph. Islands and the increase in width in the channel at the fieldsite provide areas where velocity slows, creating backwater areas where I collected samples. Riffle samples are located in fast, shallow water.

Method	# of Samples	Purpose
Bulk Sampling	21	Characterize grain size distributions
Freeze Cores	13	Collect samples at depth for metal analysis
Infiltration Bags	9	Assess infiltration rates over the course of one hydrograph after creating pore space
TSS Waterbottle	1	Collect suspended sediment over the course of one hydrograph for metal analysis

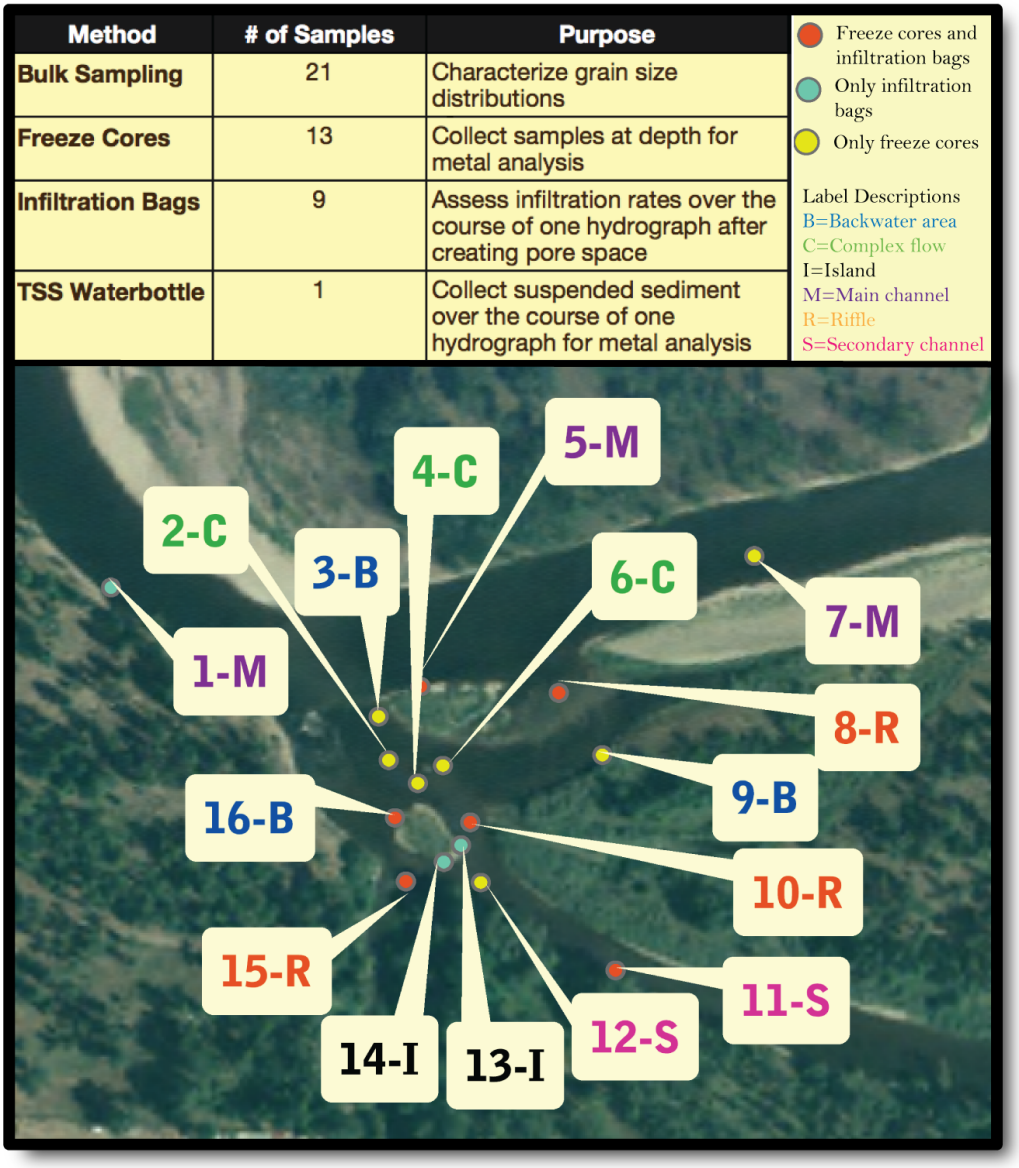

Figure 5. Sample location map. The letters next to each sample number are given to characterize primary depositional setting. Methods are described in the table in the upper third of the figure.

2.1 Tracer Rocks

Seven kilograms of small (~4mm) red gravel and 18 kilograms of large (~16-32) fluorescently painted gravel were placed in the main channel and in the riffle adjacent to the main channel prior to runoff. The high visibility of these rocks provided for a qualitative investigation of bed

mobility. The movements of these rocks complement the infiltration bag installation in determining which parts of the bed were mobile over the course of the study.

2.2 Bulk Sampling

Bulk sampling was used to characterize the grain size distribution of the substrate, including the fine sediment fraction and the variation in grain size of larger substrate, which dictates the pore space available to infiltration. Bulk samples were collected with a McNeil sampler (Shirazi and Seim, 1981; McNeil and Ahnell, 1964) to a depth of ~20 to 40 cm. The McNeil sampler is worked into the substrate until the base of the basin is level with the bed. Grains that are at least 50% enclosed in the McNeil are scooped by hand over the lip of the McNeil and into the basin within the sampler creating a circular pit approximately 26 cm wide and 15 cm deep. When the sample is collected, a lid is placed on top of the inner opening and the McNeil is removed. Two of these samples are taken within one meter of each other to constitute one sample. Sample weights have ranged from 21 to 32 kg.

Bulk samples were sieved for grain size distributions with a Ro-Tap at half-phi intervals (64 to .063 millimeters, 4 to -6 phi) to determine size distributions, D_{50}, and geometric mean and standard deviation. I used grain size distribution data to estimate porosity and available pore space using an equation developed by Wooster et al., (2008): $\lambda_p = 0.621\sigma_g^{-0.659}$, where λ_p is the porosity of sediment based upon the standard deviation σ_g of the sediment's grain size distribution from the bulk samples. This equation was derived from porosity measurements of sediments that were subsequently sieved for grain size distributions. Using a direct water saturation method after Bear (1972), Wooster et al. (2008) measured the pore space of 35

samples, finding a range of 0.25 to 0.55. The samples were sieved for grain size distributions and the standard deviation of these samples ranged between 1.2 and 3.06. The authors caution the equation is derived from specific flume sediments. Wooster et al. (2008) further stated that the applicability of this equation to natural systems is unknown. With this in mind, I applied this relationship to the field site. I calculated pore space using the geometric standard deviation of the grain size distributions.

Another issue with bulk samples in the field site is the ability of a few large particles to skew the distributions. A review of sample sizes by Church et al. (1987a) suggested that the largest clast constitute 0.1% of the sample. Sampling in this way in the field site would alter the bed enough to drive localized deposition, obscuring FSI variation across depositional settings. Adams and Beschta (1980) found that excluding rocks larger than 51mm led to less variance in percentages of fine sediment within a riffle. For this reason, I also looked at truncated grain size distributions where grains larger than 64 mm, 32 mm and 16 mm are removed and distributions calculated.

2.3 Freeze Cores

Freeze cores were used to acquire samples for metal analysis to investigate the depth and stratigraphy of infiltration. Thirteen freeze core samples were collected in 2010. A tri-axial freeze corer was used following the method of (Everest et al., 1980). To collect a sample, the triaxial freeze core sample poles were pounded as deep as possible (30 to 60 cm) into the substrate, and liquid nitrogen was inserted to freeze sediment to the pole of the injection rods (Fig. 6). The sample was removed using a tripod and come-along. Sample lengths varied between 30 and 70 cm. Sections were scooped into bags at 10 cm intervals as the sample melted. Fine sediment was then analyzed for metal content as described below.

Figure 6. Photo of freeze core equipment in place. To collect the sample, pressurized nitrogen from the nitrogen tank was inserted into the injection rods. The nitrogen cooled the water surrounding the poles, freezing the sample to the poles. The tripod and come-along, hanging over the nitrogen injection rods, were then used to remove the sample from the bed.

2.4 Infiltration Bags

Thirteen infiltration bags were installed and nine were recovered. Infiltration bags created a void for fines infiltration (Lisle and Eads, 1991) and were installed to compare infiltration across depositional settings. Spatially distributing these bags enabled investigation of infiltration of void space and variation across depositional settings.

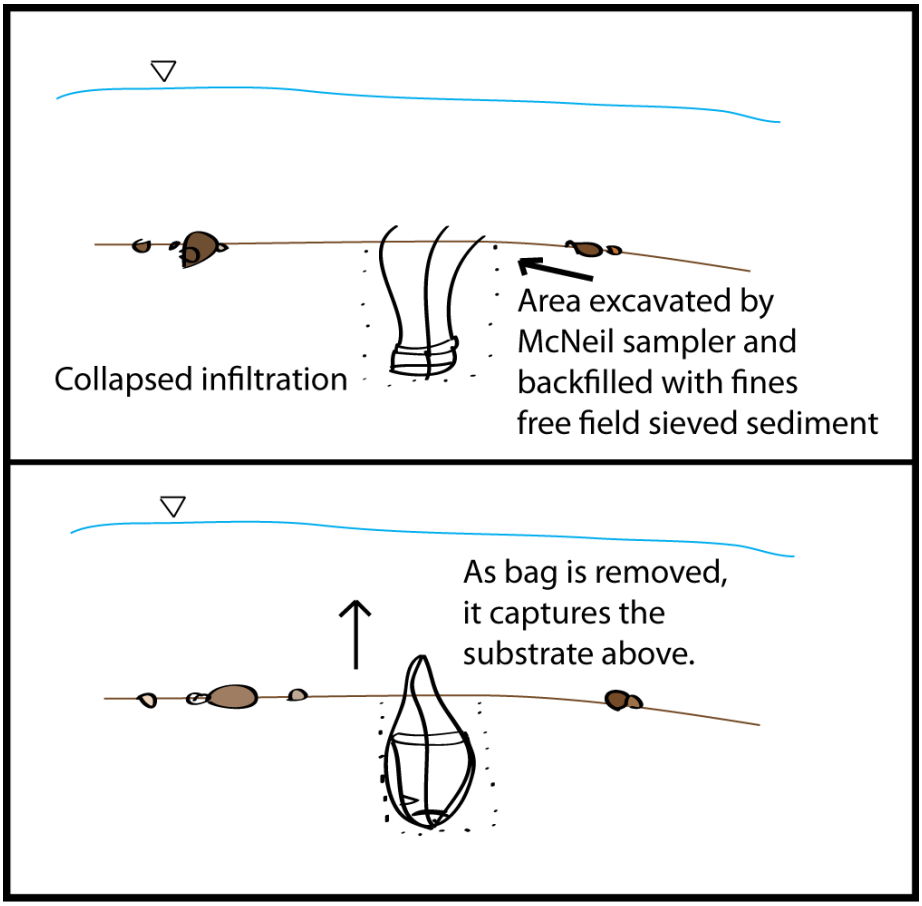

Figure 7. Infiltration bag diagram. The bed is excavated to remove fine sediment. The infiltration bag is installed and large sediment is backfilled on top of the infiltration bag. After time has elapsed, the infiltration bag is removed, capturing the sediment that has infiltrated since installation.

To install infiltration bags, a bulk sample was collected with the McNeil Sampler leaving a circular excavation pit. After the sample was removed, the McNeil was left in place to maintain the pit while the sample was field sieved. During field sieving fines (< 2mm) were removed and bagged. Larger grains were returned to a bucket and mixed. An infiltration bag was placed, collapsed, within the excavation pit (Fig. 7). Ropes were pinned onto the lip of the McNeil sampler, as coarse grains were poured over the collapsed bag in the excavation pit. The McNeil sampler was removed and ropes floated above the excavation site. Bags were spatially distributed by depositional setting in the main channel, side channels, riffles, and pools (Fig. 5).

2.5 Suspended Sediment in Transport

To collect suspended sediment in transport through the study site, two 1000 mL Nalgene bottles were connected with zip ties to 2m poles that were pounded into the bed of the river. Each bottle was affixed with a lid containing a plastic elbow that funneled a small portion of the flow (~3 mm^3) into the bottle where sediment settled out of suspension and water exited through another hole on the top of the bottle. In this manner, samples from the bottle capture sediment in transport for metal analysis over the course of the hydrograph. Three poles with a total of six bottles were installed but only one bottle was recovered.

2.6 Metal Discharge

Metal flux for sediment and water out of the reservoir has been monitored at the USGS Clark Fork above Missoula Gage 12340500 throughout remediation efforts. Parameters measured include dissolved and recoverable metal concentrations for metals of interest, suspended sediment, discharge and the percent of suspended sediment smaller than 0.063mm. Subtracting the metal concentration in the water from the total metal concentration provides the metal concentration in the sediment fraction. When this measurement is combined with the suspended sediment discharge, the sediment load for a particular metal can be calculated. The metal discharge and sediment flux for peak flows was used to constrain the timing of the metal signature found from field methods downstream.

2.7 Metal Methods and Quality Assurance/Quality Control

Seventy-six samples were analyzed for As, Cu, Pb and Zn. Nine samples came from infiltration bags. One sample came from a water bottle that collected suspended sediment samples over the

course of the 2010 water year. Thirteen freeze cores were collected. Freeze cores were sampled at 10 cm intervals to provide a stratigraphic analysis of FSI and these comprised most of the samples (62/76).

Fine sediment (<2mm) from bulk, freeze core, infiltration bag and suspended sediment samples was analyzed for metal content using Inductively Coupled Argon Plasma Optical Emission Spectrometry (ICP-OES) at the University of Montana (UM) Environmental Biogeochemistry Lab (EBL) using standard operating procedures (SOP). Samples were oven dried for 24 hours and thoroughly mixed. A portion of each sample was ground using a ball mill in a zircon vial. 0.4 g of sample was then acid digested using a modification of EPA Method 3050B (U.S. Environmental Protection Agency, 1996) during which all elements of interest in metals contaminated sediment are dissolved in solution. Elements in solution include those absorbed to mineral surfaces, tied to organic compounds and within metal oxides, hydroxides and sulfides.

SOP include the use of blanks, duplicates and spikes for quality assurance and quality control methods in order to determine instrument bias and precision. All blanks were less than .1 mg/L (n=11). Method duplicates (n=4) and lab duplicates (n=10) tested within 10% error. Average laboratory duplicates (n=10) measured to nominal concentrations were As 5.7%, Cu 1.9%, Pb 2.0% and Zn 2.3%. The Standard Reference Material (SRM) 2710 (Montana Soil) used to test accuracy had a low bias. (NIST, 2002). The laboratory spike recovery was 100% for As, 105% for Cu, 92% for PB and 91% for Zn. Average method spike to nominal concentrations was 4.6% for As, 6.2% for Cu, 7.2% for Pb and 4.8% for Zn.

3. Results

3.1 Grain size distributions

The average geometric mean for all bulk samples was 36 mm with an average geometric standard deviation of 4.1. In general, larger geometric mean grain sizes occurred in samples from the main channel (Fig. 8 A). Riffles had lower geometric standard deviations and backwater areas had higher geometric standard deviations (Fig. 8B). Smaller geometric mean grain sizes tended to have smaller standard deviations but there was no linear relationship (Fig. 8A,B).

Fine sediment fractions of truncated bulk samples were also calculated for each sample and averaged by depositional setting (Table 1)(Fig 9). Backwater areas had the highest fine sediment fraction and riffles had the lowest fine sediment fraction. Main channel and complex flow had intermediate fine sediment fractions.

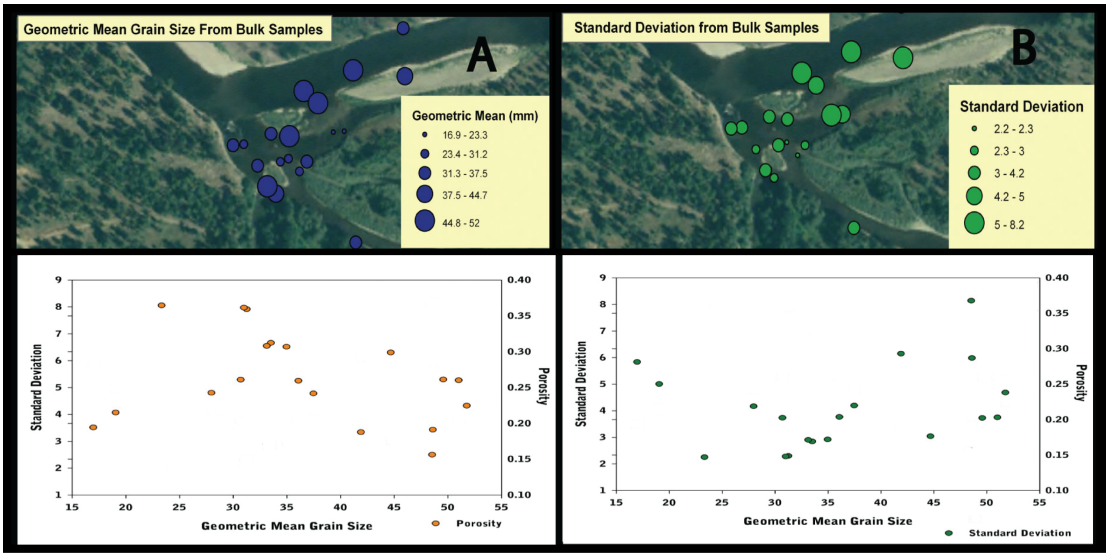

Figure 8. Location of bulk samples and associated average geometric mean grain size and standard deviation of grain size. There is symmetry within the plot because porosity is derived according to the Wooster et al. equation based upon standard deviation.

Table 1. Fine sediment fraction (<2mm) for each depositional area. Bulk samples were truncated at 64, 32 and 16 mm because larger grains may skew grain size distributions obscuring relative fine sediment fractions.

Truncation	Backwater	Main	Riffle	Complex
16 mm	39	28	15	24
32 mm	17	18	8	12
64mm	10	7	4	6

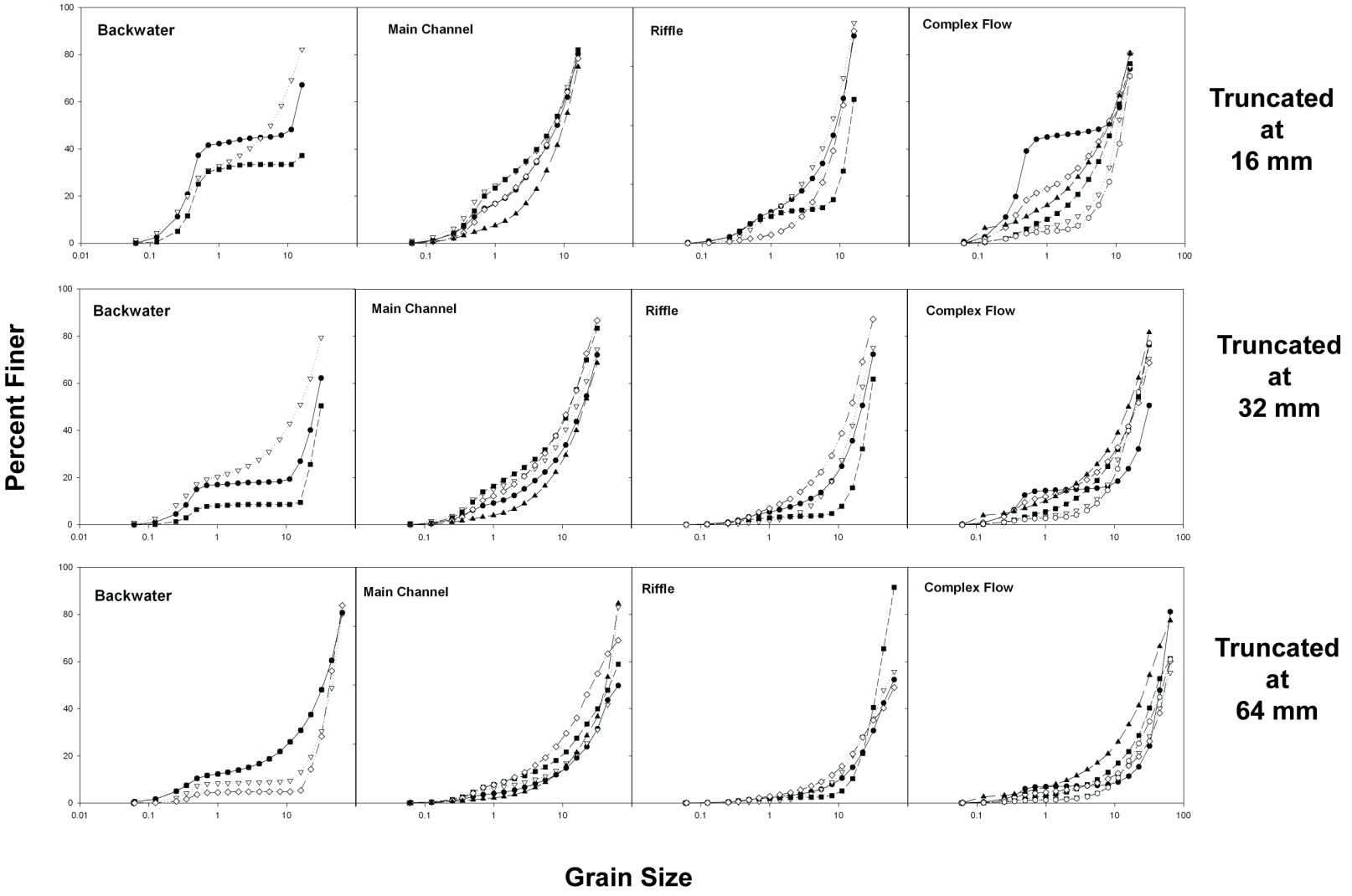

Figure 9. Grain size distributions grouped by depositional settings when bulk samples were truncated at 16, 32 and 64mm and the larger grain sizes removed. The lines are the grain sizes for each individual sample and these samples are grouped by setting according to Figure 5. Additional sampling sites not identified in Figure 5 are included here.

3.2 Metal Concentration Results from Field Samples

As a whole, the freeze core samples averaged lower metal concentrations than infiltration bags and the water bottle sample. Mean metal concentrations increased from freeze core samples to infiltration bags with the water bottle consistently reporting the highest metal concentrations (Fig. 10).

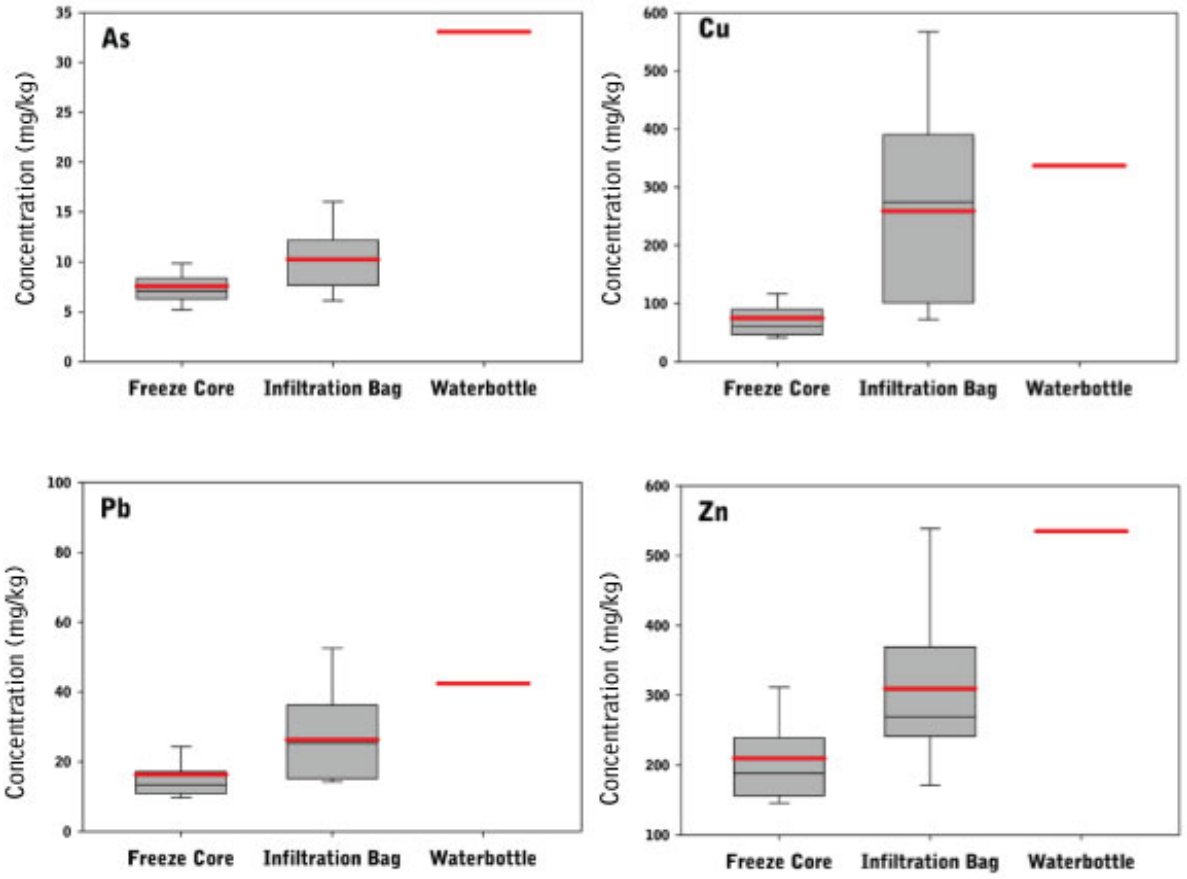

Figure 10. Metal concentrations averaged by collection method. The box represents the 25th to 75th percentile with whiskers identifying the 5th to 95th percentile. The gray line is the average and the red line is the median. The water bottle collected sediment in suspension while the infiltration bags collected sediment deposited on the bed of the river during the 2010 year. Freeze core samples were collected at depth and are not constrained in time.

Multiple sample collection methods captured fine sediment at varying temporal scales. The water bottle and infiltration bags were only in place during the 2010 hydrograph and capture fine sediment that was in transport (bottle) or depositing (bags) only during this timeframe. Alternatively, freeze core and bulk samples collect sediment that must have been deposited at some unconstrained time prior to sampling (Table 2).

Table 2. Average metal concentration (mg/kg) in sampled sediments, number of samples and time constraint on sample grouped by sample method. The sample methods with an indefinite sample time period, bulk and freeze core have similar average metal concentrations. Water year (WY) 2010 samples have higher average metal concentrations and represent sediment in transport or deposited during 2010.

Averages	As	Cu	Pb	Zn	Sample #	Sample Time
Total Average	8.39	102	18.1	230	76	
Std Dev	*4.65*	*99.0*	*12.0*	*88.9*		
Bulk	8.51	70.0	13.8	216	4	Indefinite
Std Dev	*14.5*	*145*	*14.4*	*182*		
Freeze Core	7.34	81.0	16.7	211	62	Indefinite
Std Dev	*1.80*	*30.0*	*10.8*	*60.0*		
Infiltration Bag	13.3	214	25.2	323	9	WY 2010
Std Dev	*9.30*	*198*	*16.2*	*154*		
Waterbottle *	33	337	42	535	1	WY 2010

Freeze core averages varied by sample and within each sample by depth (Fig. 11). Metal concentrations also differed due to transport and the specific dispersive and transport characteristics of each metal. Freeze cores are grouped by depositional setting and demarked by dashed lines in Figure 11. The metals concentration data shown in Figure 11 do not show patterns by depositional setting.

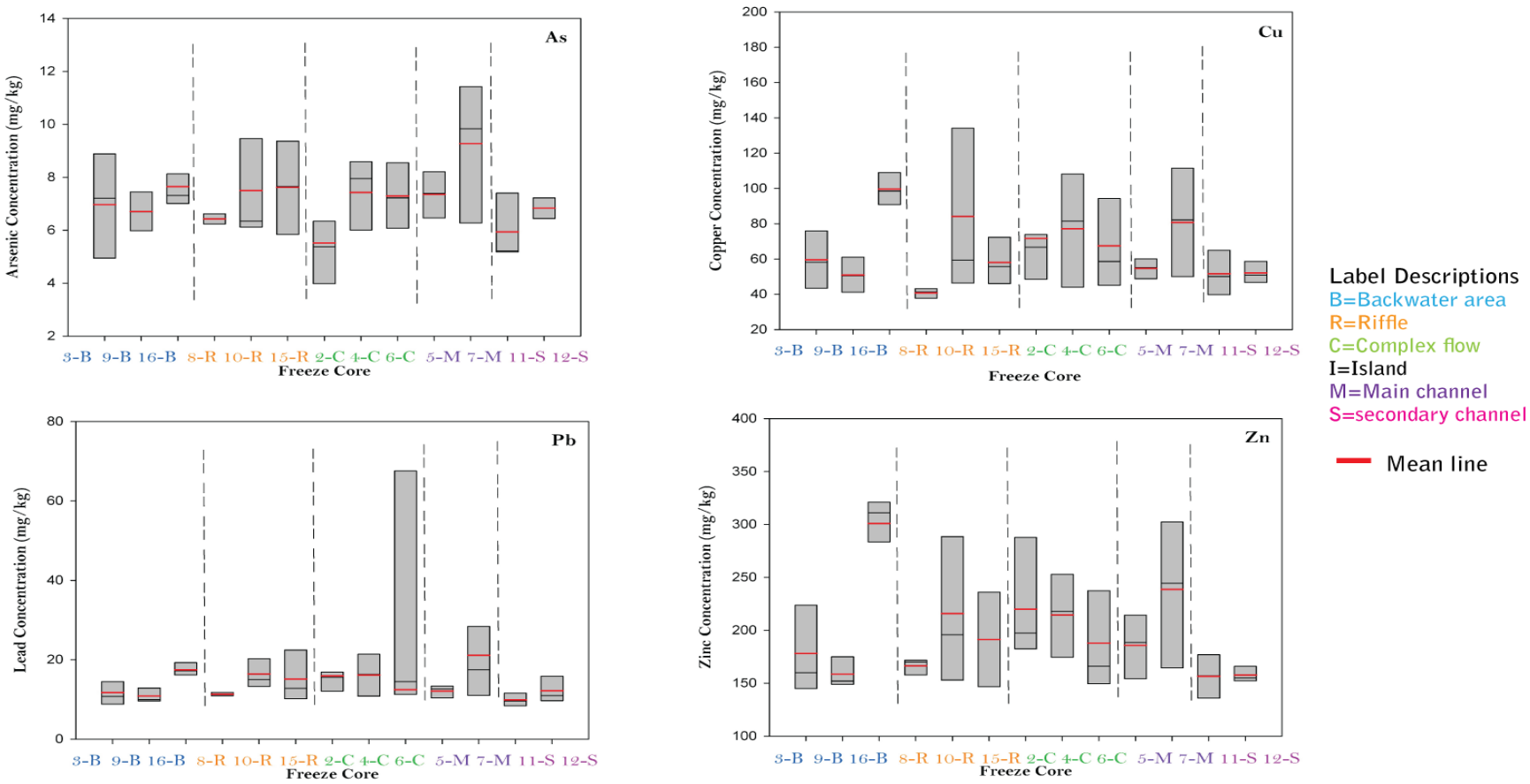

Figure 11. Box includes 25th to 75th percentile with gray line indicating average and red line showing the median. Small sample size eliminated use of whiskers. Freeze core boxplots are then grouped by depositional setting demonstrating the array both within samples and depositional settings.

Freeze core samples give metal concentrations at 10 cm intervals, providing stratigraphic comparison of infiltrated fine-grained sediment at depth (Fig. 12, 13). The freeze core samples were grouped by depositional area to determine if depositional area is a primary factor regulating the deposition of fine-grained sediment during a sediment pulse (Fig. 12, 13). The backwater areas do not share a common metal concentration stratigraphy. The riffle areas associated with the secondary channel as it flows around an island (15-R, 10-R) have a distinct peak in metal concentration 10-20 cm deep. The complex flow samples (6-C, 2-C, 4-C) do not have distinctive patterns but vary at depth. The main channel samples (7-M, 3-M) have slightly lower metal concentrations than the secondary channel sample (11-S).

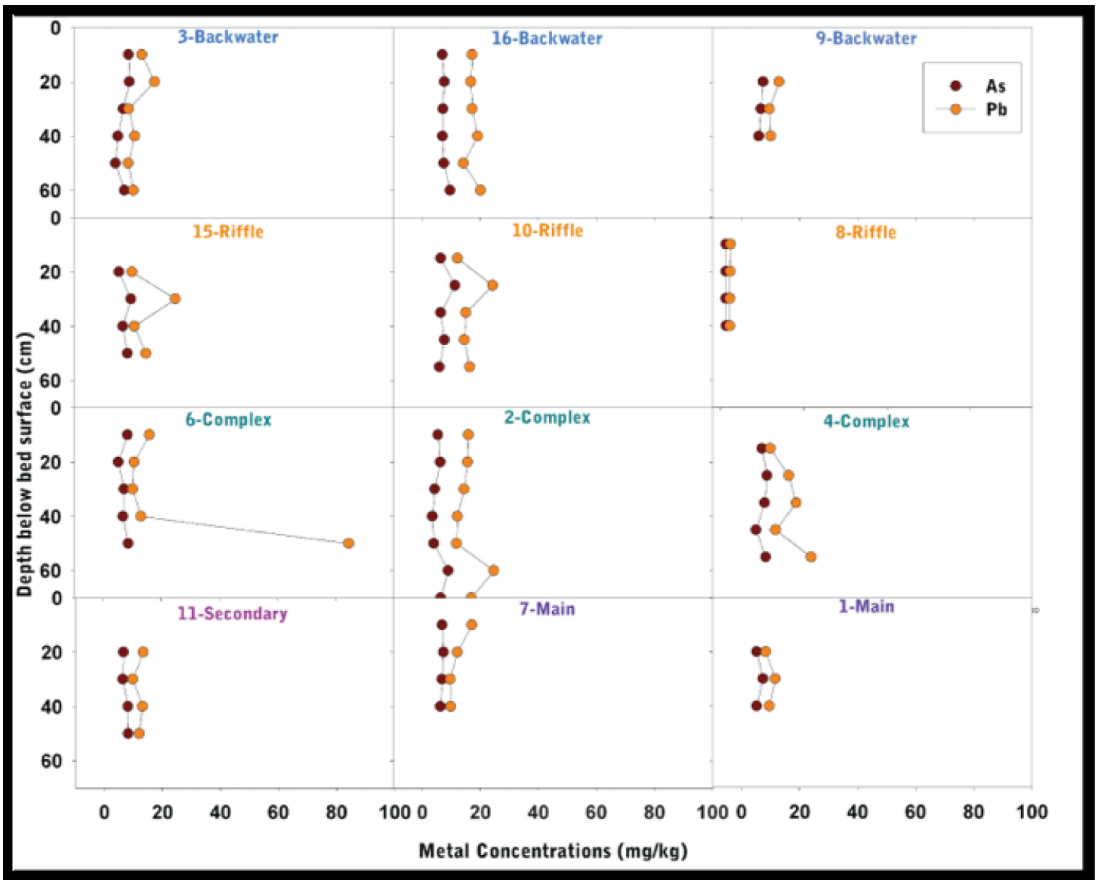

Figure 12. Freeze core metal concentration profiles grouped by depositional setting. Each line represents the metal concentration as it varies at depth in the substrate. Riffles and complex flow areas have more variation at depth.

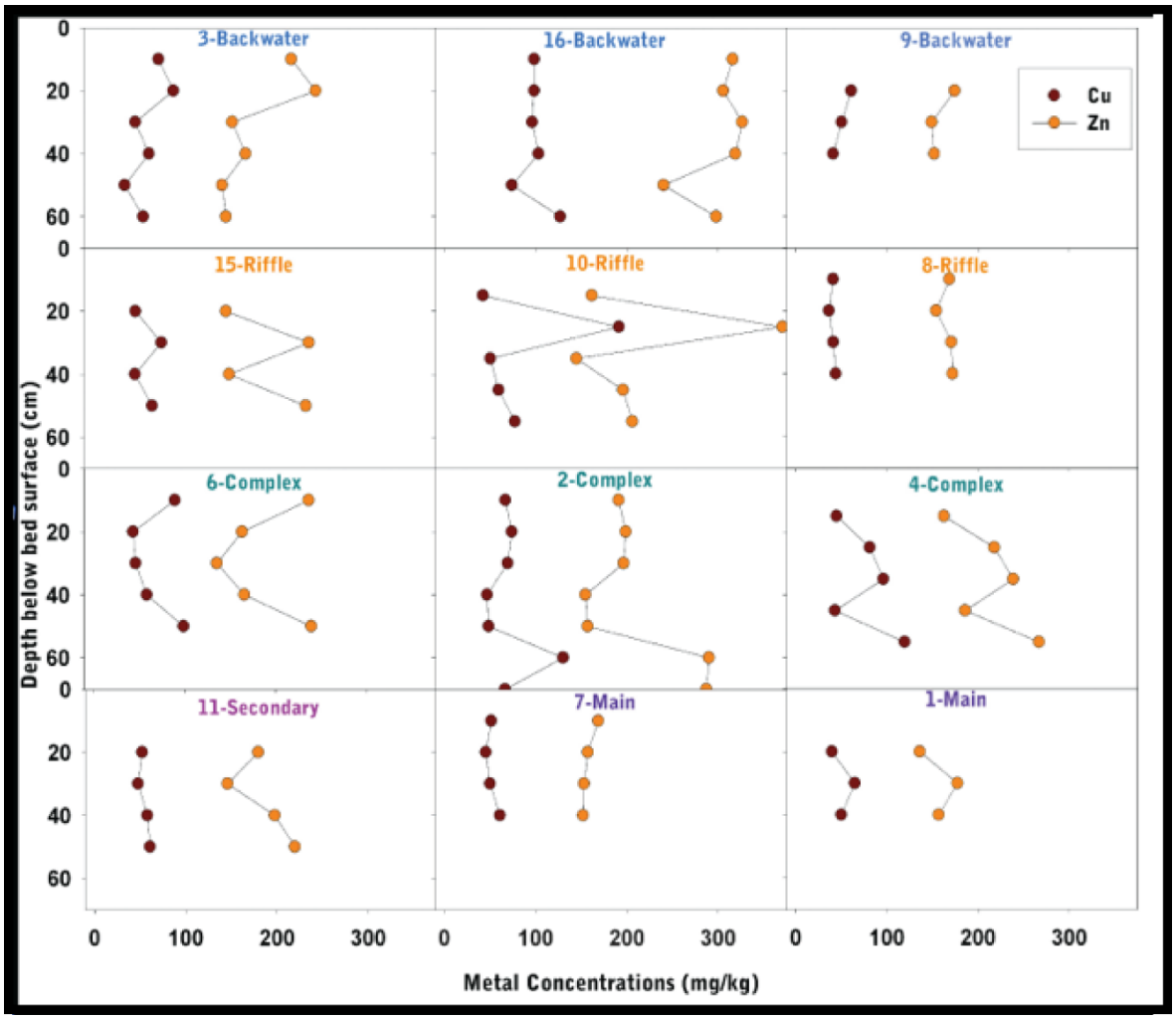

Figure 13. Freeze core metal concentration profiles grouped by depositional setting. Each line represents the metal concentration as it varies at depth in the substrate. Riffles and complex flow areas have more variation at depth.

4. Discussion

My hypotheses were: 1) Infiltrated sediment in the bed of the study reach originated from the sediment pulse produced by the removal of the Milltown dam. 2) FSI varies by depositional setting and is highest in recirculation zones associated with bifurcations and confluences in multi-thread channels. 3) Once fines have infiltrated, fine sediment in the substrate has multi-year residence times.

To assess whether infiltrated sediment in the bed came from the sediment pulse (hypothesis 1), the temporal sensitivity of the methods and analysis is important. Equally influential is the timing of the transport of metal-contaminated sediment out of Milltown reservoir. The presence of metal contaminated sediment with the As, Cu, Pb and Zn metal signature from the reservoir on the floodplain and downstream, based on other University of Montana testing, indicates that reservoir sediment moved through the field site. If the sediment deposited on the banks and floodplains was in the bed, similar metal concentrations should be found. Instead, elevated metal concentrations are absent from the substrate samples in the study. Since the sediment moved through the field site, the lack of signal must be a function of sorting, dilution of metal-contaminated sediment with uncontaminated sediment from upstream or deposition of metal contaminated sediment with subsequent reworking.

The timing of sediment transport is critical to understanding the role sorting, dilution and reworking have on sediment deposition. Metal concentrations are higher in reservoir sediments than upstream sediments transported through the reservoir. In order to use the metal

concentrations of the samples to identify the timing of infiltration, the metal concentrations and the variability of these concentrations over time need to be distinguished. As base flows did not contribute much to the transport of contaminated material to the field site, these will be ignored. Instead, I focus on periods of metal load discharge as measured at the Clark Fork above Missoula Gage (#1234500). To simplify the discussion, the time since remediation began in 2006, can be partitioned into four stages comprised of high discharge, sediment and metal flux, and correspond to the annual peak flows in 2007, 2008, 2009 and 2010 (Fig. 14). For the remainder of the discussion the year will be used to refer to the peak flows and time associated with peak flow during that year. Concentrations for As, Cu, Pb, and Zn tended to follow the same trend (Fig. 3) but for the discussion I will use copper as the example (Fig. 14). 2007 encompasses the flushing of fine sediments associated with the initial, 3.7-m drawdown the previous summer. Peak copper load out of the reservoir occurred in 2008 and is almost an order of magnitude larger than 2007 (Fig. 14). Aside from 2008, the sediment and metal loads have similar relationships to discharge both before and after the dam removal. For 2010, there are only three USGS metal analyses with which to calculate sediment load. A comparison of peak discharges of copper and water in 2007 (1,609 kg/day and 237 cms respectively) versus 2010 (836 kg/day and 217 cms respectively), demonstrates metal load at similar discharges is much lower for 2010 (Table 3). This suggests that less erosion of reservoir sediment and therefore introduction of contaminated sediment occurred in 2010. The comparison further suggests that 2010 did not contribute much metal contaminated sediment compared with 2007, 2008 and 2009.

Table 3. Stages of metals transport out of Milltown Reservoir, date ranges considered, highest copper loads and associated discharge. Figure 14 further depicts the range in copper loads over the course of each stage.

Beginning Date	End Date	Highest Cu Load (Kg/Day)	Associated Discharge (cms)
Apr 23, 2007	Jun 20, 2007	1600	237
Mar 28, 2008	Jun 24, 2008	11000	419
Apr 14, 2009	Jun 24, 2009	2900	436
May 20, 2010	Jun 16, 2010	840	219

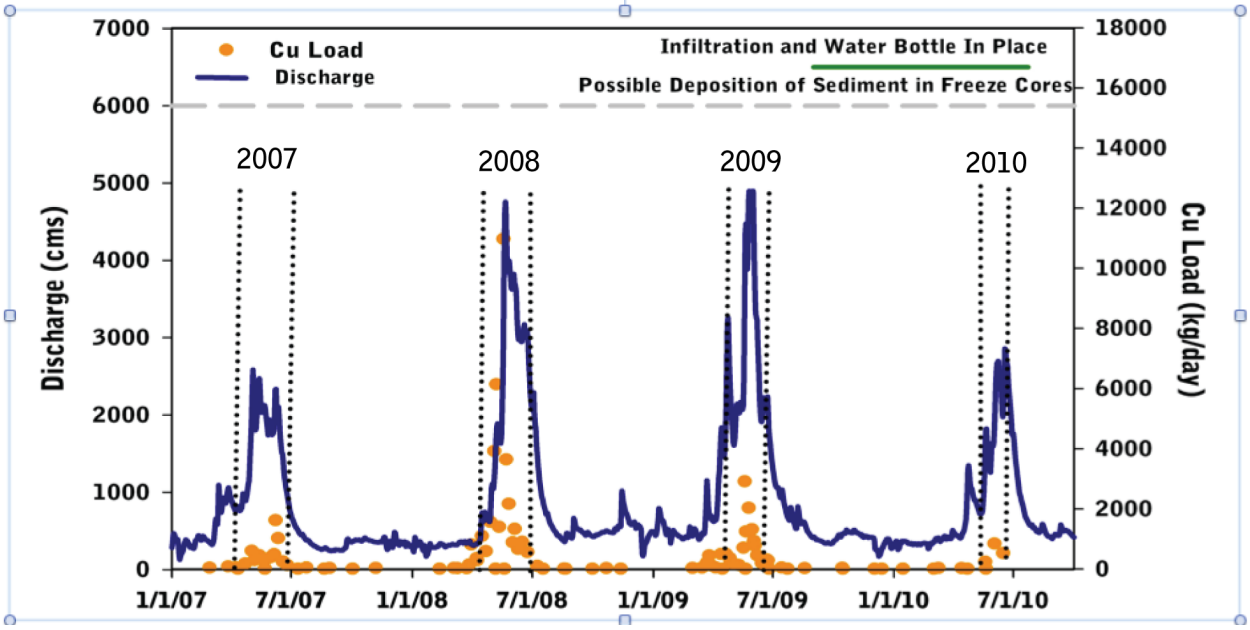

Figure 14. Plot of discharge, copper load and the duration of time the methods sample. I simplify this duration of time by demarking the periods of high discharge and metal load out of the reservoir as measured at USGS Above Missoula Gage 12340500. Each high metal load is named as a sequential stage. Metals of interest have different concentrations but generally follow the same trend. Copper and Zinc concentrations scale similarly, and are used to represent the metal load of all metals of interest out of the reservoir.

2010 is when field implementations occurred, but low peak discharge and sediment load during this stage relative to 2008 and 2009 (Fig. 14) suggest that less sediment was contributed to FSI in the field site during this time. Field evidence also suggests the bed was not reworked to the depth where the infiltration bags were installed as most of the infiltration bags installed in the bed of the river were recovered. The painted rocks on the bed of the river, however, were displaced. The substrate was reworked during 2010 flows but not at great depth. Differentiating between sediment out of the reservoir during 2009 and 2010 is not possible with USGS data due to the small number of metal load samples during 2010. For these reasons, I will continue the

discussion of metal concentrations with the interpretation that 2010 contributed little if any to the FSI and metal concentrations of samples in the field site and this sediment would be confined to the upper more mobile area of the bed.

If I compare metal concentrations from field samples to the USGS metal concentrations of 2007, 2008 and 2009, I find the field sample concentrations are within the lower bounds of 2007 and 2009. All of the samples I collected have lower concentrations than the median metal concentrations for 2008. Thus, as a whole the sediments in the field site do not reflect the large sediment pulse in 2008 that occurred following the dam breach. According to the conceptual model, I interpret this to indicate that pore space was not available when the 2008 sediment was transported through the field site. Alternatively, the substrate may have been reworked during the high flows of 2009, removing any evidence of deposition from 2008.

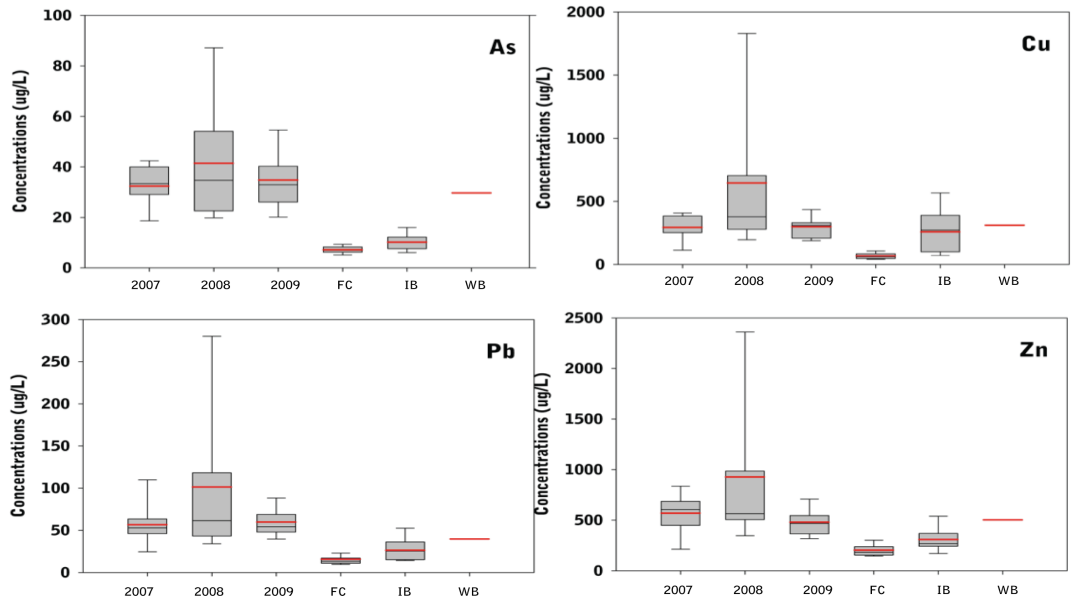

Figure 15. Box plots of metal concentrations for different time periods and field methods with box representing 25th to 75th percentile and whiskers 5th to 95th percentile. The red line represents the mean and the gray line represents the average concentrations. Freeze core samples (FC) come from different depths and are not as useful in terms of age comparison other than that they are generally lower in metal concentrations than the other metals. The water bottle (WB) and infiltration bags (IB) which sample sediment deposited during 2010 reflect metal concentrations exiting the reservoir during either 2007 or 2009 If 2008 sediments were present in the samples, concentrations would be higher. This comparison addresses hypothesis 1 by demonstrating 2008 sediments are not present within the field site.

Use of metal analysis to differentiate between samples at a finer resolution than for a comparison of years is not possible with the sample concentrations. Fine sediment for the study constitutes grains <2mm. Metals sorb to particles with larger surface areas and metal concentration is the highest on the smallest grain size fraction (Horowitz, 1984; Andrews 1987; Moore et al., 1989). A study of metal contaminated sediment in the Clark Fork River found the highest metal concentrations occurred in <300μm sediment but that notable enrichment was also found at larger size fractions (Brooke and Moore, 1988). By using the samples defined as fine sediment within this study, I was able to identify whether sediment from 2008 had infiltrated in the field site. Although samples for each method had similar fine sediment grain size distributions, inclusions of the finest fractions in some samples caused higher metal concentrations. Since slight differences in the grain size of fines can alter concentration, the ability to draw conclusions from the relatively small range of concentrations within the field samples is limited. In order to further constrain FSI timing and identify smaller scale patterns with metal concentrations, the grain size used for metal analysis would have to be uniform across all samples. In terms of using the metal concentrations out of the reservoir, the USGS samples were also collected and analyzed without differentiating grain size except for percent smaller than 0.063mm. Comparing averages of field samples with average metal concentrations out of the reservoir allows an initial comparison. Despite grain size differences if the sediment in the samples originated from the reservoir there would be greater overlap (Fig. 15).

Sorting of metal contaminated sediment in transport also likely played a large role in the distribution of metal contaminated sediment. Since the smallest sediment has more surface area to volume they have the highest concentrations. The smaller grains are also less likely than larger

grains to interact with the substrate due to hydraulic sorting and lower settling rates. Sorting could account for the overall lower metal concentrations in the field site. The location of the field site 13km downstream from the USGS-measured concentration of sediment evacuating the reservoir makes it difficult to assess the extent sorting had on distribution of metal contaminated sediments interacting with the bed despite their presence on the floodplain.

Lack of the reservoir metal signature in the samples does not mean the sediment in the reach is unrelated to the dam removal but rather that sediment dynamics involved are more complex than the release of sediment and subsequent deposition. The ramifications for remediation efforts are that metal contaminated fine sediments are transient in dynamic systems and presence of metal contaminated fines on the floodplain is not indicative of substrate composition.

To address hypothesis 2, I use grain size data supplied by bulk samples. Collecting sub-aqueous bulk samples was difficult and some fine sediment was lost. Within the sample set, however, the amount of fine sediment lost was a similar among all samples. For this reason I can compare the fine sediment fraction of the samples, acknowledging that some fines were lost from all samples. Riffles had the lowest fine sediment fraction, likely due to winnowing. Backwater samples had the highest fine sediment fraction but this may be due to deposition of lenses of fine sediment or other deposition that is not specifically FSI. Complex flow samples are a combination of processes so it is reasonable for the fine sediment fraction to reflect a combination of backwater and riffle fine sediment fractions. The similarity between complex and main channel fine sediment fractions likely reflects the location of the main channel samples, which are not in the middle of the channel. The fine sediment fraction in these samples is probably due to deposition

of finer material on the falling limb of the hydrograph. Most field studies of FSI have investigated only the riffle reaches because of the importance of these depositional areas for fish spawning (e.g., Lisle, 1989). The trend in fine sediment fraction seen in the study suggests that for a geomorphically comprehensive understanding of FSI beyond habitat importance, all depositional areas must be studied.

Another way to evaluate fine sediment fraction and identify whether FSI has already occurred would be a comparison of the porosity of the bed (e.g., using Equation 1). The range in porosity for the study was smaller, perhaps due to the larger ranges in standard deviation (Table 3). Higher standard deviation would be expected due to the larger overall grain size and large natural field setting compared to that of a flume experiment. Another possibility, however, is that FSI has occurred. FSI will create a greater range in the standard deviation of grain sizes because pores created by the large grains are now filled with smaller grains.

Table 4. Comparison of selected grain size metrics used in Wooster et al. 2008 and this study.

	Geometric Mean		Standard Deviation		Pore Space	
	Low	High	Low	High	Low	High
Montana Study	17.0	51.8	2.25	8.14	0.16	0.36
Wooster et al.	4.2	17.2	1.17	1.90	0.25	0.55

Further testing is needed but porosity measurements from grain size distributions could be an important way to expand the use of the Wooster equation in terms of predicting porosity in natural settings and to further differentiate how depositional setting affects FSI.

The large variation I found within depositional settings support Lisle's (1989) finding that transport mode, local hydraulics and channel change affect FSI at short spatial scales. The

change from single channel to multi-thread above the field site alters channel competence and affects the transport mode of sediment, especially at different points in the hydrograph. The degree of variation within depositional settings highlights the sensitivity of FSI to transport mode, local hydraulics and channel change. Hydraulic modeling would provide further insights here, as discussed in Appendix C.

Hypothesis (3) anticipates that infiltrated sediment has multi-year residence times. The similarity between the metal concentrations of 2007 and 2009 make it difficult to use these metal concentrations to differentiate between sediment from these stages. To assess this hypothesis qualitatively, I can think about deposition rates in the system. Riffle, complex, main and secondary channel depositional areas of the bed are often reworked at high flows. Backwater areas and eddies are usually not subject to scour even under high flows and are primarily depositional. Even within these depositional areas, 2008 sediments are absent. If I look at depth, the longest freeze core collected sediment from a depth of 70 cm. Erosion and reworking of larger gravel would have to occur to a depth of 70cm in order for this sediment to reflect only sediment deposited during 2009. This suggests that sediment at depth within this sample was emplaced prior to the dam removal. Multidimensional flow modeling would provide predictions of which areas of the bed were reworked under different discharges (Appendix C).

5. Conclusions

Although seen on the floodplains and banks, the high metal concentrations associated with the 2008 sediment pulse from the dam removal were not seen in the bed of the river within the field site. The goal was to examine FSI resulting from a sediment pulse of metal contaminated sediments. The metal signature from the contaminated arm of the reservoir is for the most part unseen in the bed at the field site indicating pore space was unavailable in the bed when the contaminated sediment was transported through the reach or has since been reworked. Grain size distributions from bulk sampling indicate higher fine sediment fractions occur in backwater areas with the lowest fine sediment fractions in riffles. Most field studies have focused upon riffles because of the importance to fish habitat. The study indicates riffles have the lowest fine sediment fraction. This implies FSI, especially that from fine sediment pulses, may have a larger role in shaping the geomorphology in other depositional areas. At depth and across depositional settings, fine sediment has multi-year residence times although duration may be strongly dependent upon discharge. Implications for remediation efforts are that fine sediment deposition on the banks and floodplains does not mean the substrate has been impacted, especially if pore space is already full or has been subject to reworking.

References

Adams, J.N., and Beschta, R.L., 1980, Gravel bed composition in Oregon coastal streams: Canadian Journal of Fisheries and Aquatic Sciences, v. 37, no. 10, p. 1514.

Allan, A.F., and Frostick, L., 1999, Framework dilation, winnowing, and matrix particle size; the behavior of some sand-gravel mixtures in a laboratory flume: Journal of Sedimentary Research, v. 69, no. 1, p. 21.

Andrews, E.D., 1987, Longitudinal dispersion of trace metals in the Clark Fork River, Montana: Chemical quality of water and the hydrologic cycle: Chelsea, Mich., Lewis Publishers, p. 179.

Ashley, J.T.F., Bushaw-Newton, K., Wilhelm, M., Boettner, A., Drames, G., and Velinsky, D.J., 2006, The Effects of Small Dam Removal on the Distribution of Sedimentary Contaminants: Environmental Monitoring and Assessment, v. 114, no. 1-3, p. 287.

Ashmore, P.E., 1982, Laboratory modelling of gravel braided stream morphology: Earth Surface Processes and Landforms, v. 7, no. 3, p. 201.

Ashmore, P., and Gardner, J., 2008, Unconfined confluences in braided rivers: River confluences, tributaries and the fluvial network, v. (eds S. P. Rice, A. G. Roy and B. L. Rhoads), p. 119.

Bear, J., 1972, Dynamics of fluids in porous materials: American Elsevier, New York.

Beschta, R.L., and Jackson, W.L., 1979, The intrusion of fine sediments into a stable gravel bed: Journal of the Fisheries Research Board of Canada, v. 36, no. 2.

Bluck, B.J., 1987, Bed forms and clast size changes in gravel-bed rivers: River Channels. Environment and Process. Blackwell, Oxford, p. 159.

Bridge, J.S., and Lunt, I.A., 2006, Depositional models in braided rivers: Braided rivers: process, deposits, ecology and management, p. 11.

Carling, P.A., and McCahon, C.P., 1987, Natural Siltation of Brown Trout (Salmo trutta L.) Spawning Gravels During Low-Flow Conditions: Regulated Streams: Advances in Ecology. Plenum Press, New York 1987. p 229-244.

Church, M., 2006, Bed material transport and the morphology of alluvial river channels: Annu. Rev. Earth Planet. Sci., v. 34, p. 325.

Church, M.A., McLean, D.G., and Wolcott, J.F., 1987, River bed gravels: sampling and analysis: Sediment Transport in Gravel-Bed Rivers. John Wiley and Sons New York. 1987. p 43-88.

Clifford, N.J., French, J.R., and Hardisty, J., 1993, Turbulence: Perspectives on Flow and Sediment Transport.: John Wiley & Sons.

Collins, A.L., Walling, D.E., and Leeks, G.J.L., 1996, Composite fingerprinting of the spatial source of fluvial suspended sediment: a case study of the Exe and Severn River basins, United Kingdom: Géomorphologie: relief, processus, environnement, v. 2, no. 2, p. 41.

Collins, A.L., Walling, D.E., and Leeks, G.J.L., 1997, Source type ascription for fluvial suspended sediment based on a quantitative composite fingerprinting technique: Catena, v. 29, no. 1, p. 1.

Cui, Y., Wooster, J.K., Baker, P.F., Dusterhoff, S.R., Sklar, L.S., and Dietrich, W.E., 2008, Theory of Fine Sediment Infiltration into Immobile Gravel Bed: Journal of Hydraulic Engineering, v. 134, p. 1421.

Dietrich, W.E., Kirchner, J.W., Ikeda, H., and Iseya, F., 1989, Sediment supply and the development of the coarse surface layer in gravel-bedded rivers: Nature, v. 340, no. 6230, p. 215.

Dietrich, W.E., Smith, J.D., and Dunne, T., 1979, Flow and sediment transport in a sand bedded meander: The Journal of Geology, v. 87, no. 3, p. 305.

Dingman, S.L., 2009, Fluvial Hydraulics: Oxford University Press, USA.

Diplas, P., and Parker, G., 1985, Pollution of gravel spawning grounds due to fine sediment. St. Anthony Falls Hydraulic Lab. Project Report 240: University of Minnesota, Minneapolis.

Einstein, H.A., 1968, Deposition of suspended particles in a gravel bed, *in* Journal of the Hydraulics Division, American Society of Civil Engineers, p. 1197.

Envirocon, 2004, Remedial Design Data summary Report #1, Milltown Reservoir Sediments Site Prepared by Envirocon, Inc. for the Atlantic Richfield Company.

Epstein, J.A., 2009, Upstream Geomorphic Response to Dam Removal: The Blackfoot River, Montana, unpublished thesis (M.S.), The University of Montana.

Everest, F.H., McLemore, C.E., and Ward, J.F., 1980, An improved tri-tube cryogenic gravel sampler.: Notes.

Foster, I.D.L., and Charlesworth, S.M., 1996, Heavy metals in the hydrological cycle: trends and explanation: Hydrological processes, v. 10, no. 2, p. 227.

Frings, R.M., Kleinhans, M.G., and Vollmer, S., 2008, Discriminating between pore-filling load and bed-structure load: a new porosity-based method, exemplified for the river Rhine: Sedimentology, v. 55, no. 6, p. 1571.

Frostick, L.E., Lucas, P.M., and Reid, I.A., 1984, The infiltration of fine matrices into coarse-grained alluvial sediments and its implications for stratigraphical interpretation: Journal of the Geological Society, v. 141, no. 6, p. 955.

Gibson, S., Abraham, D., Heath, R., and Schoellhamer, D., 2009, Vertical gradational variability of fines deposited in a gravel framework: Sedimentology, v. 56, no. 3, p. 661.

Greig, S.M., Sear, D.A., and Carling, P.A., 2005, The impact of fine sediment accumulation on the survival of incubating salmon progeny: Implications for sediment management: Science of the Total Environment, v. 344, no. 1-3, p. 241.

Gruszowski, K.E., Foster, I.D.., Lees, J.A., and Charlesworth, S.M., 2003, Sediment sources and transport pathways in a rural catchment, Herefordshire, UK: Hydrological Processes, v. 17, no. 13, p. 2665.

Horowitz, A.J., 1984, A primer on trace metal-sediment chemistry: Geolog. Surv. Water-Supply Paper.

Ikeda, H., 1984, Flume experiments on the transport of sand-gravel mixtures: Bulletin of the Environmental Research Center, University of Tsukuba, v. 8, p. 1.

Johns, C., and Moore, J.N., 1985, Metals in the bottom sediments of the lower Clark Fork River reservoirs: Montana Water Resources Research Center.

Johnsen, J., 2011, Sampling and Modeling of Sediment Transport and Reservoir Erosion Following Dam Removal: Milltown Dam, Montana, unpublished thesis (M.S.), The University of Montana.

Keller, E., 1972, Development of alluvial stream channels: a five-stage model: Geological Society of America Bulletin, v. 83, no. 5, p. 1531.

Kirchner, J.W., Dietrich, W.E., Iseya, F., and Ikeda, H., 1990, The variability of critical shear stress, friction angle, and grain protrusion in water-worked sediments: Sedimentology, v. 37, no. 4, p. 647.

Kleinhans, M.G., 2010, Sorting out river channel patterns: Progress in Physical Geography, v. 34, no. 3, p. 287.

Kleinhans, M.G., and Van Rijn, L.C., 2002, Stochastic prediction of sediment transport in sand-gravel bed rivers: Journal of Hydraulic Engineering, v. 128, p. 412.

Lambing, J.H., Sando, S.K., Agency, U.S.E.P., and (US), G.S., 2009, Estimated Loads of Suspended Sediment and Selected Trace Elements Transported Through the Milltown Reservoir Project Area Before and After the Breaching of Milltown Dam in the Upper Clark Fork Basin, Montana, Water Year 2008: US Geological Survey.

Leonardson, R., 2010, Exchange of fine sediments with gravel riverbeds, unpublished thesis (PhD), The University of California-Berkeley.

Lisle, T.E., 1989, Sediment transport and resulting deposition in spawning gravels, north coastal California: Water Resources Research, v. 25, no. 6, p. 1303.

Lisle, T., and Eads, R., 1991, Methods to Measure Sedimentation of Spawning Gravels: Forest Service, Pacific Southwest Research Station, Research Note PSW-411.

Lisle, T.E., and Hilton, S., 1999, Fine bed material in pools of natural gravel bed channels: Water Resources Research, v. 35, no. 4, p. 1291.

Martin, J.M., and Meybeck, M., 1979, Elemental mass-balance of material carried by major world rivers: Marine Chemistry, v. 7, no. 3, p. 173.

McNeil, W.J., and Ahnell, W.H., 1964, Success of pink salmon spawning relative to size of spawning bed materials: US Fish and Wildlife Service.

Moore, J.N., and Landrigan, E.M., 1999, Mobilization of metal-contaminated sediment by ice-jam floods: Environmental Geology, v. 37, no. 1, p. 96.

Moore, J.N., and Luoma, S.N., 1990, Hazardous wastes from large-scale metal extraction. A case study: Environmental science & technology, v. 24, no. 9, p. 1278.

Moore, J.N., Ficklin, W.H., and Johns, C., 1988, Partitioning of arsenic and metals in reducing sulfidic sediments: Environmental science & technology, v. 22, no. 4, p. 432.

Mosley, M.P., 1976, An experimental study of channel confluences: The Journal of Geology, v. 84, no. 5, p. 535.

Orsic, I., In Progress, Downstream Deposition of Contaminated Sediment Following the Removal of Milltown Dam, Montana, unpublished thesis (M.S.), The University of Montana.

Paola, C., 1989, A simple basin-filling model for coarse-grained alluvial systems: Quantitative Dynamic Stratigraphy,, p. 363.

Parker, G., Seminara, G., and Solari, L., 2003, Bed load at low Shields stress on arbitrarily sloping beds: Alternative entrainment formulation: Water Resour. Res, v. 39, no. 7, p. 1183.

Prandtl, L., 1925, Report on investigation of developed turbulence: Mechanik, v. 5, no. 2.

Richards, C., and Bacon, K.L., 1994, Influence of fine sediment on macroinvertebrate colonization of surface and hyporheic stream substrates: Western North American Naturalist, v. 54, no. 2, p. 106.

Ridgway, K., and Tarbuck, K.J., 1968, Voidage fluctuations in randomly-packed beds of spheres adjacent to a containing wall: Chemical Engineering Science, v. 23, no. 9, p. 1147.

Sakthivadivel, R., and Einstein, H.A., 1970, Clogging of porous column of spheres by sediment: Journal of the Hydraulics Division, v. 96, no. 2, p. 461.

Salomons, W., 1995, Environmental impact of metals derived from mining activities: processes, predictions, prevention: Journal of Geochemical Exploration, v. 52, no. 1-2, p. 5.

Sear, D.A., 1993, Fine sediment infiltration into gravel spawning beds within a regulated river experiencing floods: ecological implications for salmonids: Regulated Rivers: Research & Management, v. 8, no. 4, p. 373.

Shankar, R., Thompson, R., and Galloway, R.B., 1994, Sediment source modelling: Unmixing of artificial magnetisation and natural radioactivity measurements: Earth and Planetary Science Letters, v. 126, no. 4, p. 411.

Shirazi, M.A., and Seim, W.K., 1981, Stream system evaluation with emphasis on spawning habitat for salmonids: Water Resources Research, v. 17, no. 3, p. 592.

Slattery, W., Christy, B., Carmody, B., and Gales, B., 2002, Effects of composted feedlot manure on the chemical characteristics of duplex soils in north-eastern Victoria: Australian journal of experimental agriculture, v. 42, no. 3, p. 369.

Standish, N., and Borger, D.E., 1979, The porosity of particulate mixtures: Powder Technology, v. 22, no. 1, p. 121.

Sulaiman, M., Tsutsumi, D., Fujita, M., and Hayashi, K., 2007, Classification of grain size distribution curves of bed material and the porosity: 京都大学防災研究所年報. B= Disaster Prevention Research Institute Annuals. B, v. 50, no. B, p. 615.

Suttle, K.B., Power, M.E., Levine, J.M., and McNeely, C., 2004, How fine sediment in riverbeds impairs growth and survival of juvenile salmonids: Ecological Applications, v. 14, no. 4, p. 969.

Thompson, D.M., Nelson, J.M., and Wohl, E.E. Interactions between pool geometry and hydraulics: Water Resources Research, v. 34, no. 12.

Titan, 1995, Milltown Reservoir Sediments Operable Unit, Final Draft Remedial Investigation Report: Prepared by Titan Environmental Corporation for the Atlantic Richfield Company V. 1-3.

U.S. Environmental Protection Agency, 2004, Milltown Res- Reservoir Sediments Operable Unit of the Milltown Reservoir/ Clark Fork River Superfund Site—Record of Decision, Part 2: Decision Summary.

Venditti, J.G., Dietrich, W.E., Nelson, P.A., Wydzga, M.A., Fadde, J., and Sklar, L., 2010, Effect of sediment pulse grain size on sediment transport rates and bed mobility in gravel bed rivers: J. Geophys. Res, v. 115.

Vollmer, S., and Kleinhans, M.G., 2007, Predicting incipient motion, including the effect of turbulent pressure fluctuations in the bed: Water Resour. Res, v. 43.

Walden, J., Slattery, M.C., and Burt, T.P., 1997, Use of mineral magnetic measurements to fingerprint suspended sediment sources: approaches and techniques for data analysis: Journal of Hydrology, v. 202, no. 1-4, p. 353.

Wallbrink, P., Martin, C., and Wilson, C., 2003, Quantifying the contributions of sediment, sediment-P and fertiliser-P from forested, cultivated and pasture areas at the landuse and catchment scale using fallout radionuclides and geochemistry: Soil and tillage research, v. 69, no. 1-2, p. 53.

Walling, D.E., and Woodward, J.C., 1995, Tracing sources of suspended sediment in river basins: a case study of the River Culm, Devon, UK: Marine and Freshwater Research, v. 46, no. 1, p. 327.

Walling, D.E., Collins, A.L., and McMellin, G.K., 2003, A reconnaissance survey of the source of interstitial fine sediment recovered from salmonid spawning gravels in England and Wales: Hydrobiologia, v. 497, no. 1, p. 91.

Wilcox, A.C., Brinkerhoff, D., and Woelf-Erskin, C., 2009, Initial geomorphic responses to removal of Milltown Dam, Clark Fork River, Montana, USA: Eos Trans. AGU, v. 89(53).

Wooster, J.K., Dusterhoff, S.R., Cui, Y., Sklar, L.S., Dietrich, W.E., and Malko, M., 2008, Sediment supply and relative size distribution effects on fine sediment infiltration into immobile gravels: Water Resour. Res, v. 44.

A. Grain Size Data Appendix

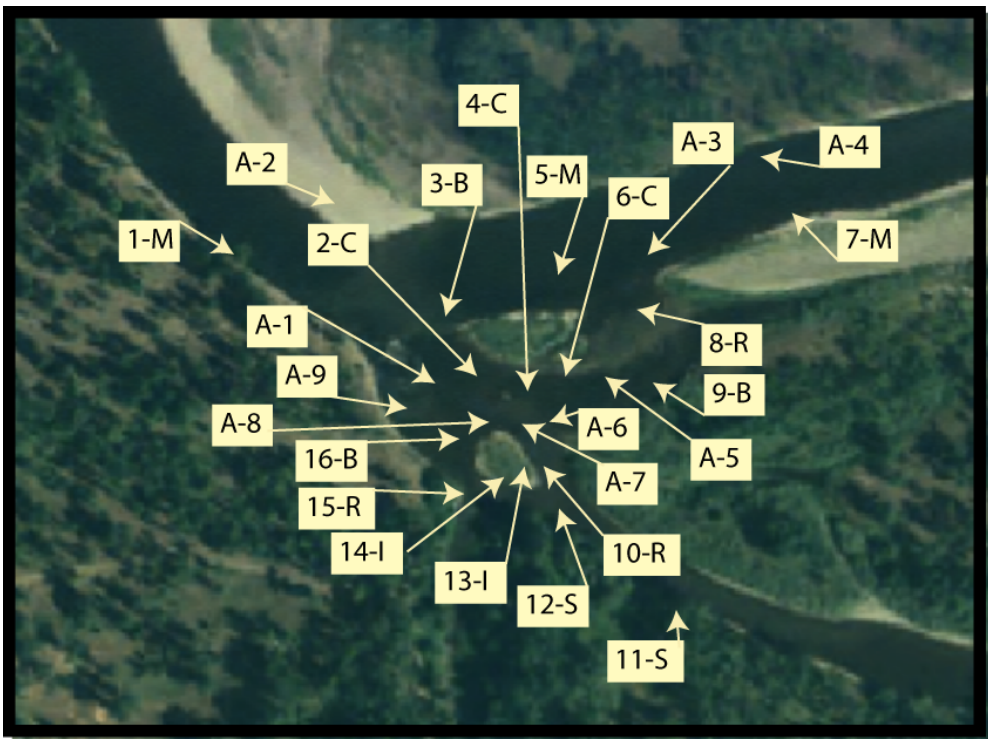

Figure 16-A. The locations of samples are identified above. Locations used for samples in the main body of the thesis are marked with a number and letter. Additional bulk sample locations names begin with an A.

Table 6-A. Grain size distribution of sediment. Weight is in kilograms.

Sample name	A-7	2-C	4-C	A-8	6-C	A-6	1-M
	Complex					Other	
>64	4.42	10.13	7.94	9.33	5.01	5.01	7.7
>45	7.79	3.44	1.72	5.13	2.06	2.06	7.63
>32	5.53	2.69	2.55	2.8	1.32	1.32	1.96
>22.4	2.07	1.6	2.38	1.51	1.2	1.2	1.03
>16	0.94	1.21	1.39	0.9	0.94	0.94	0.82
>11.2	0.59	1.08	1.01	0.79	0.93	0.93	0.75
>8	0.25	0.97	0.79	0.54	0.52	0.52	0.58
>5.6	0.08	0.56	0.64	0.4	0.32	0.32	0.42
>4	0.03	0.26	0.44	0.28	0.18	0.18	0.27
>2.8	0.03	0.18	0.37	0.23	0.11	0.11	0.23
>2	0.02	0.11	0.27	0.17	0.05	0.05	0.18
>1.4	0.02	0.07	0.21	0.14	0.02	0.02	0.14
>1	0.02	0.04	0.15	0.1	0.01	0.01	0.13
>0.7	0.04	0.02	0.1	0.08	0.01	0.01	0.12
>0.5	0.18	0.03	0.14	0.14	0.02	0.02	0.2
>0.35	0.69	0.09	0.14	0.3	0.04	0.04	0.33
>0.25	0.31	0.09	0.1	0.24	0.04	0.04	0.21
>0.125	0.3	0.08	0.09	0.22	0.04	0.04	0.17
>.062	0.07	0.02	0.02	0.06	0.01	0.01	0.07
<.062	0.03	0.01	0.01	0.02	0.01	0.01	0.05
Total	23.42	22.65	20.45	23.38	12.83	12.83	22.99

*All samples are bulk samples unless signified by a depth, for example 10-20, which indicates freeze core or by IB, infiltration bag.

Table 7-A. Grain size distribution of sediment in smaller samples from infiltration bags and portions of freeze cores. Weight is in kilogram

Sample name	16-B IB	10-R IB	15-R 0-10	1-M IB	15-R IB	12-S IB	15-R 21-30	15-R 31-40	15-R 11-20	10-R 40	10-R 30	15-R IB
>64	0.00	0.00	0.00	0.77	2.51	0.00	0.64	1.91	0.63	2.56	0.00	0.00
>45	1.03	1.02	0.00	0.30	0.38	0.77	0.14	0.22	0.16	0.00	0.00	0.02
>32	0.06	0.00	0.20	0.13	0.00	0.45	0.30	0.49	0.19	0.00	0.11	0.02
>22.4	0.07	0.16	0.01	0.21	0.13	0.06	0.37	0.36	0.12	0.00	0.11	0.05
>16	0.01	0.14	0.01	0.04	0.11	0.04	0.23	0.19	0.07	0.00	0.06	0.06
>11.2	0.06	0.18	0.01	0.10	0.13	0.03	0.14	0.12	0.02	0.03	0.05	0.04
>8	0.06	0.10	0.01	0.03	0.04	0.01	0.10	0.09	0.02	0.01	0.04	0.06
>5.6	0.04	0.09	0.02	0.02	0.02	0.01	0.06	0.09	0.02	0.00	0.03	0.04
>4	0.03	0.07	0.01	0.02	0.01	0.01	0.03	0.04	0.01	0.00	0.02	0.02
>2.8	0.01	0.03	0.01	0.00	0.00	0.01	0.03	0.03	0.01	0.00	0.01	0.01
>2	0.01	0.01	0.01	0.00	0.00	0.00	0.03	0.02	0.01	0.00	0.01	0.00
>1.4	0.01	0.01	0.00	0.00	0.00	0.00	0.03	0.03	0.01	0.00	0.03	0.00
>1	0.01	0.01	0.00	0.00	0.00	0.00	0.02	0.04	0.01	0.00	0.00	0.00
>0.7	0.00	0.01	0.00	0.00	0.00	0.00	0.02	0.05	0.01	0.00	0.00	0.00
>0.5	0.04	0.02	0.00	0.00	0.06	0.02	0.05	0.17	0.02	0.01	0.48	0.00
>0.35	0.00	0.00	0.00	0.00	0.00	0.00	0.00	0.00	0.00	0.00	0.00	0.00
>0.25	0.05	0.02	0.00	0.01	0.07	0.03	0.01	0.02	0.00	0.01	0.14	0.01
>0.125	0.03	0.02	0.00	0.02	0.10	0.03	0.01	0.01	0.00	0.01	0.20	0.01
>.062	0.01	0.01	0.00	0.01	0.04	0.01	0.00	0.00	0.00	0.00	0.09	0.00
<.062	0.00	0.01	0.00	0.00	0.02	0.00	0.00	0.01	0.00	0.00	0.04	0.00
Total	1.53	1.90	0.29	1.66	3.60	1.47	2.22	3.89	1.31	2.63	1.42	0.71

*All samples are bulk samples unless signified by a depth, for example 10-20, which indicates freeze core or by IB, infiltration bag.

Table 8-A. Grain size distribution of sediment in infiltration bags. Weight is in kilograms.

Sample name	10-R IB	8-R IB	5-M IB	16-B IB	1-M IB	11-S IB	7-M IB
>64	1.74	1.16	0.69	0.00	0.63	1.22	0.98
>45	0.00	0.00	0.73	0.85	0.99	0.47	0.00
>32	0.19	0.22	0.29	0.35	0.00	0.27	0.15
>22.4	0.21	0.14	0.08	0.44	0.07	0.03	0.11
>16	0.05	0.06	0.09	0.14	0.00	0.09	0.04
>11.2	0.04	0.03	0.04	0.04	0.00	0.05	0.04
>8	0.02	0.02	0.03	0.05	0.00	0.04	0.04
>5.6	0.03	0.02	0.02	0.02	0.00	0.03	0.02
>4	0.02	0.01	0.01	0.02	0.00	0.02	0.02
>2.8	0.01	0.00	0.00	0.01	0.00	0.00	0.00
>2	0.01	0.00	0.00	0.00	0.00	0.00	0.00
>1.4	0.01	0.00	0.00	0.00	0.00	0.00	0.00
>1	0.00	0.00	0.00	0.00	0.00	0.00	0.00
>0.7	0.00	0.00	0.00	0.00	0.00	0.00	0.00
>0.5	0.00	0.01	0.00	0.01	0.00	0.00	0.00
>0.35	0.00	0.00	0.00	0.02	0.00	0.00	0.00
>0.25	0.00	0.00	0.00	0.03	0.00	0.00	0.00
>0.125	0.00	0.00	0.00	0.03	0.00	0.00	0.00
>.062	0.00	0.00	0.00	0.01	0.00	0.00	0.00
<.062	0.00	0.00	0.00	0.01	0.00	0.00	0.00
Total	2.35	1.68	1.99	2.03	1.70	2.22	1.41

*All samples are bulk samples unless signified by a depth, for example 10-20, which indicates freeze core or by IB, infiltration bag.

Table 9-A Geometric mean grain size, standard deviation of the grain size distribution, and porosity of the sample (calculated using Equation 1). Location information is in Figure 1.

Bulk Sample	Geometric Mean	Standard Deviation	Calculated Pore Space
A-1	28.0	4.2	0.24
A-7	30.7	3.7	0.26
A-4	35.0	2.9	0.31
A-3	48.6	8.1	0.16
5-M	48.6	6.0	0.19
7-M	41.9	6.1	0.19
A-6	44.7	3.0	0.30
8-R	51.0	3.7	0.26
A-6	37.5	4.2	0.24
A-2	23.3	2.2	0.36
A-8	36.1	3.8	0.26
A-5	33.5	2.8	0.31
1-M	31.3	2.3	0.36
9-B	19.1	5.0	0.22
15-R	49.6	3.7	0.26
10-R	31.0	2.3	0.36
A-9	17.0	5.8	0.19
5-M	51.8	4.7	0.23
16-B	33.1	2.9	0.31

Bulk Sample Comparison

For primary results, bulk and infiltration samples were used (data above). Pebble counts were also conducted but not as frequently as bulk samples. To identify sampling bias, I compared pebble counts to bulk and infiltration bag grain size data.

Pebble Counts

Wolman pebble counts will be used to assess surficial grain size distribution (M. G Wolman, 1954). The counts are conducted by randomly walking in a zig-zag pattern in a patch of the river that is qualitatively the same. Every two strides the finger is blindly put directly down to select the grain directly under the finger. The intermediate axis, perpendicular to the a-axis, is

measured and recorded. One hundred measurements are made providing randomized point measurements.

Sediment Size Distribution Results

Sediment size distribution was calculated for bulk samples, pebble counts, infiltration bags and field sieving. Bulk samples and infiltration bags were dried and sieved. Field sieving was not dried before sieving and thus is biased by incorporated water weight and smaller grains sticking to larger grains. High uncertainty in the results of field sieving has led to those being excluded from grain size distribution results.

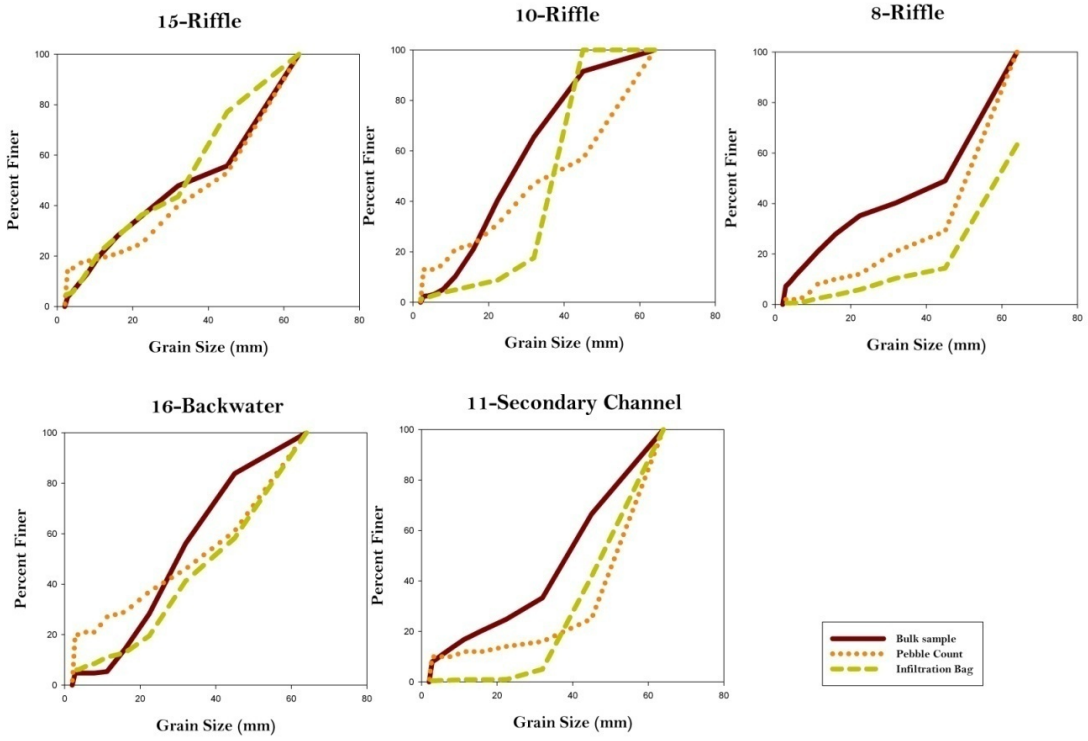

Figure 17-A. Bulk, infiltration bag and pebble counts were compiled into percent finer tables to identify trends in grain size distributions based upon collection method. Results demonstrate general trends captured by all methods.

B. Metal Discharge and Analysis Appendix

Metal Discharge Data

Table 10-B. Data from USGS Above Missoula Gage 1234500 used to calculate metal load out of Milltown dam and reservoir. Samples without metal load are included as part of the larger USGS data set.

Date	Time	Discharge, instantaneous cfs	Discharge (L/day)	Arsenic, water filtered ug/L	Arsenic, water, unfiltered, ug/L	Copper, water, filtered, ug/L	Copper, water, unfiltered, recoverable, ug/L	Lead, water, filtered, ug/L	Lead, water, unfiltered, recoverable, ug/L	Zinc, water, filtered, ug/L	Zinc, water, unfiltered, recoverable, ug/L	Suspended sediment, % smaller than 0.063 mm	Suspended sediment concentration, mg/L	Suspended sediment discharge, tons/day	Arsenic Residual Sed Conc (ug/L)	Arsenic Sed Conc (ug/g)	Copper Residual Sed Conc (ug/L)	Copper Sed Conc (ug/g)	Lead Residual Sed Conc (ug/L)	Lead Sed Conc (ug/g)	Zinc Residual Sed Conc (ug/L)	Zinc Sed Conc (ug/g)	Sed As Load (kg/day)	Sed Cu Load (kg/day)	Sed Pb Load (kg/day)	Sed Zn Load (kg/day)
6/13/06	14:30	6900	1.69E+10	4.7	8.6	3.3	42.1	0.12	6.89	2.6	91	39	117	2180	3.9	33	38.8	332	6.8	58	88	756	65.8	655.07	114.3	1492.48
6/19/06	15:00	4720	1.15E+10	3.1	6.6	1.8	9.9	0.08	1.25	3.2	12	40	47	599	3.5	74	8.1	172	1.2	25	9	187	40.4	93.55	13.51	101.63
6/22/06	15:15	4040	9.89E+09												0								0	0	0	0
6/26/06	14:00	3050	7.46E+09	3.2	4	1.6	17.7	0.1	1.6	2	19	61	26	214	0.8	31	16.1	619	1.5	58	17	654	6	120.15	11.19	126.87
7/19/06	13:00	1600	3.92E+09												0								0	0	0	0
7/25/06	16:15	1320	3.23E+09	3.6	4.2	2	14.6	0.08	1.98	1.2	21	81	12	43	0.6	50	12.6	1050	1.9	158	20	1650	1.9	40.7	6.14	63.95
8/25/06	9:10	873	2.14E+09	3	3.3	1.7	8.1	0.04	0.97	2.8	12	85	11	26	0.3	27	6.4	582	0.9	85	9	836	0.6	13.67	1.99	19.65
9/26/06	15:00	1090	2.67E+09	4.8	6.2	2	17.7	0.13	2.73	1.7	36	78	27	79	1.4	52	15.7	581	2.6	96	34	1270	3.7	41.87	6.93	91.48
10/17/06	14:00	1350	3.30E+09	4.8	7.4	3	27.9	0.12	5.18	4	60	70	47	171	2.6	55	24.9	530	5.1	108	56	1191	8.6	82.25	16.71	184.98
11/7/06	15:10	1630	3.99E+09												0								0	0	0	0
11/15/06	10:00	2130	5.21E+09	3.2	3.6	1.2	7.9	0.12	1.09	3	15	37	18	104	0.4	22	6.7	372	1	54	12	667	2.1	34.92	5.06	62.54
2/28/07	8:45	1230	3.01E+09	3.8	4.4	1.8	12.8	0.07	1.71	3.6	18	65	10	33	0.6	60	11	1100	1.6	164	14	1440	1.8	33.11	4.94	43.34
3/28/07	15:00	3760	9.20E+09	2.3	3.3	1.6	9.6	0.12	1.98	1.7	22	14	100	1020	1	10	8	80	1.9	19	20	203	9.2	73.6	17.11	186.76

Date	Time	Discharge, instantaneous cfs	Discharge (L/day)	Arsenic, water filtered ug/L	Arsenic, water, unfiltered, ug/L	Copper, water, filtered, ug/L	Copper, water, unfiltered, recoverable, ug/L	Lead, water, filtered, ug/L	Lead, water, unfiltered, recoverable, ug/L	Zinc, water, filtered, ug/L	Zinc, water, unfiltered, recoverable, ug/L	Suspended sediment, % smaller than 0.0063 mm	Suspended sediment concentration, mg/L	Suspended sediment discharge, tons/day	Arsenic Residual Sed Conc (ug/L)	Arsenic Sed Conc (ug/g)	Copper Residual Sed Conc (ug/L)	Copper Sed Conc (ug/g)	Lead Residual Sed Conc (ug/L)	Lead Sed Conc (ug/g)	Zinc Residual Sed Conc (ug/L)	Zinc Sed Conc (ug/g)	Sed As Load (kg/day)	Sed Cu Load (kg/day)	Sed Pb Load (kg/day)	Sed Zn Load (kg/day)
4/9/07	15:00	2800	6.85E+09	2.9	3.6	1.7	8.4	0.12	1.91	1.9	15	38	32	242	0.7	22	6.7	209	1.8	56	13	409	4.8	45.9	12.26	89.75
4/12/07	11:00	2990	7.32E+09																				0	0	0	0
4/23/07	14:30	3010	7.37E+09	3.6	6.1	2.2	25.4	0.07	4.39	2.2	54.4	42	68	553	2.5	37	23.2	341	4.3	64	52	768	18.4	170.87	31.82	384.45
5/3/07	15:30	8560	2.09E+10	2.4	8.1	2	30.4	0.07	6.53	2.9	52.8	28	281	6490	5.7	20	28.4	101	6.5	23	50	178	119.4	594.84	135.3	1045.16
5/7/07	11:30	6540	1.60E+10	2.7	4.8	2.3	20	0.1	3.6	2.4	37.8	56	70	1240	2.1	30	17.7	253	3.5	50	35	506	33.6	283.24	56.01	566.48
5/14/07	15:00	8890	2.18E+10	2.6	4.9	2.1	22.9	0.12	3.99	2.5	47	34	126	3020	2.3	18	20.8	165	3.9	31	45	353	50	452.45	84.18	967.99
5/22/07	14:30	7580	1.85E+10	2.4	4	1.8	15.4	0.12	2.47	2.4	25.3	47	51	1040	1.6	31	13.6	267	2.4	46	23	449	29.7	252.24	43.59	424.73
5/23/07	16:45	8000	1.96E+10																				0	0	0	0
5/31/07	16:30	6390	1.56E+10	4.5	7	2.7	26.5	0.12	4.05	2.4	45	49	62	1070	2.5	40	23.8	384	3.9	63	43	687	39.1	372.12	61.45	666.07
6/6/07	14:30	7200	1.76E+10	4.1	7.2	2.3	29.5	0.12	5.05	3.2	56.5	39	93	1810	3.1	33	27.2	292	4.9	53	53	573	54.6	479.19	86.85	939
6/8/07	8:15	8370	2.05E+10	8.1	16.7	7.4	86	0.33	14.1	6	140	44	200	4520	8.6	43	78.6	393	13.8	69	134	670	176.1	1609.74	282.01	2744.34
6/12/07	15:00	7620	1.86E+10	6.7	12.1	4.3	58.9	0.08	9.06	3.5	104	39	160	3290	5.4	34	54.6	341	9	56	101	628	100.7	1018.02	167.43	1873.82
6/19/07	15:30	5390	1.32E+10	5.2	7	2.5	20.7	0.12	3.14	3.3	40.8	29	62	902	1.8	29	18.2	294	3	49	38	605	23.7	240.03	39.83	494.57
6/20/07	7:20	4440	1.09E+10	5.1	7.1	2.6	23.2	0.07	6.07	2.9	45.5	43	50	599	2	40	20.6	412	6	120	43	852	21.7	223.8	65.18	462.81
6/26/07	13:00	4070	9.96E+09	4.5	5.4	1.8	13.5	0.06	1.69	2.6	23.1	29	40	440	0.9	23	11.7	293	1.6	41	21	513	9	116.52	16.23	204.15
7/12/07	14:45	1740	4.26E+09																				0	0	0	0
7/25/07	8:40	1320	3.23E+09	3.6	4	1.9	13.9	0.08	1.73	2	16.9	81	12	43	0.4	33	12	1000	1.7	138	15	1242	1.3	38.76	5.33	48.12

Date	Time	Discharge, instantaneous cfs	Discharge (L/day)	Arsenic, water filtered ug/L	Arsenic, water, unfiltered, ug/L	Copper, water, filtered, ug/L	Copper, water, unfiltered, recoverable, ug/L	Lead, water, filtered, ug/L	Lead, water, unfiltered, recoverable, ug/L	Zinc, water, filtered, ug/L	Zinc, water, unfiltered, recoverable, ug/L	Suspended sediment, % smaller than 0.0063 mm	Suspended sediment concentration, mg/L	Suspended sediment discharge, tons/day	Arsenic Residual Sed Conc (ug/L)	Arsenic Sed Conc (ug/g)	Copper Residual Sed Conc (ug/L)	Copper Sed Conc (ug/g)	Lead Residual Sed Conc (ug/L)	Lead Sed Conc (ug/g)	Zinc Residual Sed Conc (ug/L)	Zinc Sed Conc (ug/g)	Sed As Load (kg/day)	Sed Cu Load (kg/day)	Sed Pb Load (kg/day)	Sed Zn Load (kg/day)
8/21/07	16:30	1040	2.54E+09																				0	0	0	0
8/29/07	7:45	873	2.14E+09	4.1	4.6	1.9	11.7	0.1	1.85	2.7	19.8	76	14	33	0.5	36	9.8	700	1.8	125	17	1221	1.1	20.93	3.74	36.53
10/3/07	16:30	1320	3.23E+09																				0	0	0	0
11/7/07	11:00	1270	3.11E+09	3.9	4.9	1.4	8.5	0.04	1.15	3.1	15.7	67	7	24	1	143	7.1	1014	1.1	159	13	1800	3.1	22.06	3.45	39.15
2/12/08	14:35	1200	2.94E+09																				0	0	0	0
3/5/08	9:10	1160	2.84E+09	3.7	4.7	2.2	9.5	0.05	1.79	4	13.8	74	9	28	1	111	7.3	811	1.7	193	10	1089	2.8	20.72	4.94	27.82
3/10/08	14:00	1170	2.86E+09	3.8	4.9	2.3	8.9	0.06	1.42	3.8	14.8	73	13	41	1.1	85	6.6	508	1.4	105	11	846	3.1	18.89	3.89	31.49
3/24/08	15:30	1180	2.89E+09	6.3	9.2	7	11.1	0.45	1.87	7.4	19.9	84	27	86	2.9	107	4.1	152	1.4	53	13	463	8.4	11.84	4.1	36.09
3/28/08	13:50	1560	3.82E+09	4	9.3	1.8	37.8	0.07	7.35	3.1	94.9	80	180	758	5.3	29	36	200	7.3	40	92	510	20.2	137.41	27.79	350.41
3/31/08	15:00	1100	2.69E+09	6.4	19.7	4.2	303	0.64	42.5	6.4	404	84	127	377	13.3	105	298.8	2353	41.9	330	398	3131	35.8	804.23	112.67	1070.15
4/8/08	16:00	1160	2.84E+09	5.9	11.5	3.6	126	0.4	20.5	3.6	170	84	87	272	5.6	64	122.4	1407	20.1	231	166	1913	15.9	347.41	57.05	472.3
4/9/08	14:00	1170	2.86E+09	5.6	10.4	3.5	102	0.26	15.8	4.2	130	82	58	183	4.8	83	98.5	1698	15.5	268	126	2169	13.7	281.99	44.49	360.14
4/16/08	16:00	2510	6.14E+09	6	20.8	4.9	182	0.33	32	5.5	258	55	247	1670	14.8	60	177.1	717	31.7	128	253	1022	90.9	1087.68	194.5	1550.75
4/22/08	15:10	2350	5.75E+09	4.1	9.9	2.5	104	0.21	16.1	3.4	143	39	147	933	5.8	39	101.5	690	15.9	108	140	950	33.4	583.63	91.37	802.71
4/29/08	15:30	3170	7.76E+09	5	16.4	4.1	205	0.41	30.6	7.3	289	36	325	2780	11.4	35	200.9	618	30.2	93	282	867	88.4	1558.28	234.17	2185.01
5/5/08	15:15	4640	1.14E+10	5.2	22.5	4.5	349	0.87	53.5	4.2	444	25	557	6980	17.3	31	344.5	618	52.6	94	440	790	196.4	3911.24	597.53	4993.21
5/7/08	17:00	6440	1.58E+10																					0	0	0

Date	Time	Discharge, instantaneous cfs	Discharge (L/day)	Arsenic, water filtered ug/L	Arsenic, water, unfiltered, ug/L	Copper, water, filtered, ug/L	Copper, water, unfiltered, recoverable, ug/L	Lead, water, filtered, ug/L	Lead, water, unfiltered, recoverable, ug/L	Zinc, water, filtered, ug/L	Zinc, water, unfiltered, recoverable, ug/L	Suspended sediment, % smaller than 0.0063 mm	Suspended sediment concentration, mg/L	Suspended sediment discharge, tons/day	Arsenic Residual Sed Conc (ug/L)	Arsenic Sed Conc (ug/g)	Copper Residual Sed Conc (ug/L)	Copper Sed Conc (ug/g)	Lead Residual Sed Conc (ug/L)	Lead Sed Conc (ug/g)	Zinc Residual Sed Conc (ug/L)	Zinc Sed Conc (ug/g)	Sed As Load (kg/day)	Sed Cu Load (kg/day)	Sed Pb Load (kg/day)	Sed Zn Load (kg/day)
5/8/08	15:30	6580	1.61E+10	4.6	26.9	5	386		54	4.7	495	19	950	16900	22.3	23	381	401	54	57	490	516	359	6134.2	869.41	7893.96
5/12/08	15:00	6090	1.49E+10	3.5	10.1	2.4	95.8	0.31	14.9	2.4	134	20	333	5480	6.6	20	93.4	280	14.6	44	132	395	98.3	1391.78	217.41	1961.01
5/19/08	15:30	14800	3.62E+10	3.6	26	5.2	308	0.45	45.6	6.8	541	36	1060	42400	22.4	21	302.8	286	45.2	43	534	504	811.2	10965.4	1635.03	19345.17
5/20/08	7:15	16000	3.92E+10																					0	0	0
5/23/08	15:15	14400	3.52E+10	2.8	13	3.9	107	0.18	15.5	5.9	184	37	334	13000	10.2	31	103.1	309	15.3	46	178	533	359.4	3632.69	539.79	6275.28
5/27/08	16:00	14100	3.45E+10	3.3	9.2	4.1	66.6	0.17	9.45	5.5	100	48	272	10400	5.9	22	62.5	230	9.3	34	95	347	203.6	2156.28	320.17	3260.3
6/2/08	14:45	13300	3.25E+10	3.2	6.1	3	29.9	0.12	5.06	5.5	55.6	47	146	5240	2.9	20	26.9	184	4.9	34	50	343	94.4	875.41	160.76	1630.41
6/5/08	9:45	12900	3.16E+10	3.8	9	4	46	0.2	7.62	5.2	81.4	47	150	5220	5.2	35	42	280	7.4	49	76	508	164.1	1325.7	234.21	2405.2
6/10/08	17:00	10500	2.57E+10	4.7	7.7	3.9	29.5	0.08	5.02	5	50.1	53	80	2270	3	38	25.6	320	4.9	62	45	564	77.1	657.71	126.92	1158.7
6/16/08	16:30	10800	2.64E+10	4.6	8.9	4.7	38.4	0.19	5.66	4.8	67.4	54	89	2600	4.3	48	33.7	379	5.5	61	63	703	113.6	890.55	144.55	1654.26
6/24/08	15:30	10500	2.57E+10	4.7	7.2	3.4	24.9	0.11	3.95	3.9	42	54	68	1930	2.5	37	21.5	316	3.8	56	38	560	64.2	552.38	98.66	978.86
7/9/08	12:40	4970	1.22E+10	4.4	5.7	2.7	10.3	0.08	1.55	2.6	14.8	69	20	268	1.3	65	7.6	380	1.5	74	12	610	15.8	92.42	17.88	148.36
7/18/08	6:45	3040	7.44E+09																				0	0	0	0
8/19/08	17:40	1270	3.11E+09	3.6	4	1.5	2.5	0.08	0.18	1.8	3.3	75	3	10	0.4	133	1	333	0.1	33	2	500	1.2	3.11	0.31	4.66
8/21/08	13:25	1510	3.69E+09																				0	0	0	0
10/1/08	7:40	2550	6.24E+09																				0	0	0	0
10/1/08	13:10	1550	3.79E+09																				0	0	0	0

Date	Time	Discharge, instantaneous cfs	Discharge (L/day)	Arsenic, water filtered ug/L	Arsenic, water, unfiltered, ug/L	Copper, water, filtered, ug/L	Copper, water, unfiltered, recoverable, ug/L	Lead, water, filtered, ug/L	Lead, water, unfiltered, recoverable, ug/L	Zinc, water, filtered, ug/L	Zinc, water, unfiltered, recoverable, ug/L	Suspended sediment, % smaller than 0.0063 mm	Suspended sediment concentration, mg/L	Suspended sediment discharge, tons/day	Arsenic Residual Sed Conc (ug/L)	Arsenic Sed Conc (ug/g)	Copper Residual Sed Conc (ug/L)	Copper Sed Conc (ug/g)	Lead Residual Sed Conc (ug/L)	Lead Sed Conc (ug/g)	Zinc Residual Sed Conc (ug/L)	Zinc Sed Conc (ug/g)	Sed As Load (kg/day)	Sed Cu Load (kg/day)	Sed Pb Load (kg/day)	Sed Zn Load (kg/day)
10/22/08	11:45	1750	4.28E+09	4.2	4.7	2	6.2	0.07	1.27	2.4	8.7	82	7	33	0.5	71	4.2	600	1.2	171	6	900	2.1	17.98	5.14	26.98
11/13/08	7:40	2550	6.24E+09																				0	0	0	0
3/2/09	15:30	1650	4.04E+09	3.6	4.4	2.2	7.8	0.05	1.24	1.3	10.8	82	13	58	0.8	62	5.6	431	1.2	92	10	731	3.2	22.61	4.8	38.35
3/16/09	16:30	1720	4.21E+09	3.4	4.5	2.9	10.6	0.05	1.62	4.1	16.3	75	16	74	1.1	69	7.7	481	1.6	98	12	763	4.6	32.41	6.61	51.34
3/24/09	16:20	3320	8.12E+09	4.5	7.7	5.6	31.1	0.26	5.67	4.9	40.3	76	71	636	3.2	45	25.5	359	5.4	76	35	499	26	207.15	43.95	287.57
3/25/09	16:30	2880	7.05E+09	4.2	6.1	3.9	21.4	0.1	3.31	5.1	28.5	75	38	295	1.9	50	17.5	461	3.2	84	23	616	13.4	123.32	22.62	164.9
3/27/09	16:00	2350	5.75E+09	4.4	14.2	3.5	79.7	0.1	12.7	8.3	114	77	94	596	9.8	104	76.2	811	12.6	134	106	1124	56.4	438.16	72.45	607.78
3/31/09	16:00	2240	5.48E+09	3.9	5.9	2.4	20.7	0.07	3.23	8.1	36.9	68	25	151	2	80	18.3	732	3.2	126	29	1152	11	100.3	17.32	157.85
4/6/09	15:30	2270	5.55E+09	3.7	4.5	2.7	9.6	0.07	1.43	2.7	13.3	73	14	86	0.8	57	6.9	493	1.4	97	11	757	4.4	38.32	7.55	58.88
4/14/09	16:30	6520	1.60E+10	3.5	7.9	3.5	33.9	0.13	6.44	8	55.2	58	108	1900	4.4	41	30.4	281	6.3	58	47	437	70.2	484.98	1006.7	753
4/16/09	8:30	5870	1.44E+10																				0	0	0	0
4/21/09	16:10	7620	1.86E+10	2.5	6.3	2.6	29.1	0.09	6.14	5.9	49.8	52	126	2590	3.8	30	26.5	210	6.1	48	44	348	70.9	494.09	112.8	818.51
4/27/09	16:00	8350	2.04E+10	2.8	4.8	3.2	20.8	0.11	3.52		29.9	64	56	1260	2	36	17.6	314	3.4	61	30	534	40.9	359.59	69.67	610.89
4/29/09	12:30	7160	1.75E+10	2.4	3.9	2.6	14.8	0.15	2.96	2.9	17	64	36	696	1.5	42	12.2	339	2.8	78	14	392	26.3	213.74	49.23	247.02
5/4/09	15:25	5990	1.47E+10	2.9	4	2.5	13.1	0.07	2.3	6	19.6	68	29	469	1.1	38	10.6	366	2.2	77	14	469	16.1	155.36	32.68	199.33
5/11/09	15:30	7140	1.75E+10	2.9	3.8	2.2	9.1	0.07	1.65	2.2	12.8	65	33	636	0.9	27	6.9	209	1.6	48	11	321	15.7	120.55	27.6	185.19
5/18/09	16:15	9230	2.26E+10	2.8	5.6	2.5	33.4	0.11	5.9	2.5	47	50	111	2770	2.8	25	30.9	278	5.8	52	45	401	63.2	697.86	130.76	1005.01

Date	Time	Discharge, instantaneous cfs	Discharge (L/day)	Arsenic, water filtered ug/L	Arsenic, water, unfiltered, ug/L	Copper, water, filtered, ug/L	Copper, water, unfiltered, recoverable, ug/L	Lead, water, filtered, ug/L	Lead, water, unfiltered, recoverable, ug/L	Zinc, water, filtered, ug/L	Zinc, water, unfiltered, recoverable, ug/L	Suspended sediment, % smaller than 0.0063 mm	Suspended sediment concentration, mg/L	Suspended sediment discharge, tons/day	Arsenic Residual Sed Conc (ug/L)	Arsenic Sed Conc (ug/g)	Copper Residual Sed Conc (ug/L)	Copper Sed Conc (ug/g)	Lead Residual Sed Conc (ug/L)	Lead Sed Conc (ug/g)	Zinc Residual Sed Conc (ug/L)	Zinc Sed Conc (ug/g)	Sed As Load (kg/day)	Sed Cu Load (kg/day)	Sed Pb Load (kg/day)	Sed Zn Load (kg/day)
5/20/09	11:20	15400	3.77E+10	3	11.4	4.3	81.4	0.22	15.8	4.5	139	46	422	17500	8.4	20	77.1	183	15.6	37	135	319	316.5	2905.24	587.08	5068.16
5/21/09	9:17	15900	3.89E+10																				0	0	0	0
5/22/09	15:00	14500	3.55E+10	3.7	7.4	4.4	39.3	0.11	7.51	3.8	61.2	49	183	7160	3.7	20	34.9	191	7.4	40	57	314	131.3	1238.23	262.55	2036.51
5/26/09	15:30	17300	4.23E+10	4.6	9.2	5.6	53.4	0.14	9.36	6	96.8	59	171	7990	4.6	27	47.8	280	9.2	54	91	531	194.7	2023.4	390.29	3843.61
5/31/09	15:15	17400	4.26E+10	4	7.6	4.2	34.9	0.07	6.31	3.4	61.4	55	152	7140	3.6	24	30.7	202	6.2	41	58	382	153.3	1307.06	265.67	2469.36
6/3/09	11:10	14000	3.43E+10	4.3	7.6	4.9	31.9	0.15	4.66	5.4	57.7	64	83	3140	3.3	40	27	325	4.5	54	52	630	113	924.91	154.49	1791.58
6/4/09	17:30	12300	3.01E+10	4.5	7.2	4.3	29.7	0.1	4.55	5.6	51.4	59	82	2720	2.7	33	25.4	310	4.5	54	46	559	81.3	764.44	133.93	1378.41
6/8/09	15:00	10400	2.54E+10	4.6	6.3	4.1	21.5	0.1	3.36	5.7	32.7	61	56	1570	1.7	30	17.4	311	3.3	58	27	482	43.3	442.78	82.96	687.07
6/15/09	17:00	7220	1.77E+10	4	5.2	3	13.7	0.07	2.08	2.8	20	56	34	663	1.2	35	10.7	315	2	59	17	506	21.2	189.03	35.51	303.86
6/23/09	17:45	7800	1.91E+10	5.5	7.5	5.2	20.9	0.1	3.36	3.8	30.5	59	40	842	2	50	15.7	393	3.3	82	27	668	38.2	299.64	62.22	509.58
6/24/09	9:40	7120	1.74E+10	5.2	7.1	5	20.7	0.12	3.12	3.8	26.5	51	26	500	1.9	73	15.7	604	3	115	23	873	33.1	273.52	52.26	395.47
6/26/09	14:45	6000	1.47E+10																				0	0	0	0
7/15/09	13:25	3680	9.00E+09	4.4	4.9	2.7	6.7	0.05	0.78	1.7	8.1	68	7	70	0.5	71	4	571	0.7	104	6	914	4.5	36.02	6.57	57.63
7/24/09	11:20	2320	5.68E+09																				0	0	0	0
8/19/09	13:00	2070	5.07E+09	5.4	6.1	2.3	5.8	0.04	0.88	1.6	7.7	73	9	50	0.7	78	3.5	389	0.8	93	6	678	3.5	17.73	4.25	30.9
10/15/09	11:30	1640	4.01E+09	4.6	5.3	1.6	8.6	0.04	1.57	3.3	13.7	80	11	49	0.7	64	7	636	1.5	139	10	945	2.8	28.09	6.14	41.73
10/16/09	10:16		0.00E+00																				0	0	0	0

Date	Time	Discharge, instantaneous cfs	Discharge (L/day)	Arsenic, water filtered ug/L	Arsenic, water, unfiltered, ug/L	Copper, water, filtered, ug/L	Copper, water, unfiltered, recoverable, ug/L	Lead, water, filtered, ug/L	Lead, water, unfiltered, recoverable, ug/L	Zinc, water, filtered, ug/L	Zinc, water, unfiltered, recoverable, ug/L	Suspended sediment, % smaller than 0.0063 mm	Suspended sediment concentration, mg/L	Suspended sediment discharge, tons/day	Arsenic Residual Sed Conc (ug/L)	Arsenic Sed Conc (ug/g)	Copper Residual Sed Conc (ug/L)	Copper Sed Conc (ug/g)	Lead Residual Sed Conc (ug/L)	Lead Sed Conc (ug/g)	Zinc Residual Sed Conc (ug/L)	Zinc Sed Conc (ug/g)	Sed As Load (kg/day)	Sed Cu Load (kg/day)	Sed Pb Load (kg/day)	Sed Zn Load (kg/day)
12/3/09	8:45		0.00E+00																				0	0	0	0
12/14/09	10:50		0.00E+00																				0	0	0	0
1/15/10	8:52		0.00E+00																				0	0	0	0
3/3/10	8:19		0.00E+00																				0	0	0	0
3/10/10	14:15	1400	3.43E+09	4.6	5.5	3.8	11.3	0.05	1.66	2.9	15	87	12	45	0.9	75	7.5	625	1.6	134	12	1008	3.1	25.69	5.52	41.45
4/14/10	14:15	1630	3.99E+09	3.3	3.8	1.7	6		0.76		8.6	79	10	44	0.5	50	4.3	430	0.8	76	9	860	2	17.15	3.03	34.3
4/23/10	8:44		0.00E+00																				0	0	0	0
5/20/10	15:15	6500	1.59E+10	2.1	3.8	2.3	16.7	0.06	5.03	2.1	28.6	56	78	1370	1.7	22	14.4	185	5	64	27	340	27	229.02	79.05	421.47
5/21/10	12:15		0.00E+00																				0	0	0	0
6/3/10	14:45	7240	1.77E+10	3.5	9	3.1	50.3	0.1	8.59	3	90.8	47	134	2620	5.5	41	47.2	352	8.5	63	88	655	97.4	836.16	150.4	1555.39
6/16/10	13:35	7740	1.89E+10	4.6	8.1	3.9	31.1	0.17	5.08	3.8	44.3	63	57	1190	3.5	61	27.2	477	4.9	86	41	711	66.3	515.13	92.99	767.01

Field Sample Metal Concentration Results

Table 11-B. Sample name and concentrations (mg/kg) for metals of interest.

Sample Name	As	Cu	Pb	Zn
3-B-30-40-FC	9.18	88.8	18.0	246
Q7-10-20-FC	8.28	58.6	13.4	200
4-C-0-10-FC	8.78	101	85.9	242
9-B-0-10-FC	6.05	41.7	10.2	154
12-S-10-20-FC	11.3	94.4	22.3	287
15-R-0-10-FC	6.03	79.0	16.7	211
8-R-0-10-FC	5.33	51.5	9.90	162
12-S-21-30-FC	10.9	113	20.6	301
A-5	5.57	49.5	11.9	167
3-B-50-60-FC	9.11	74.3	13.8	225
3-B-10-20-FC	4.45	36.0	9.02	147
7-M-30-40-FC	6.85	54.2	13.9	186
8-R-20-30-FC	5.41	41.3	8.68	141
10-R-20-30-FC	6.54	52.0	15.5	149
4-C-30-40-FC	7.29	48.5	9.86	154
9-B-20-30-FC	5.05	42.1	10.3	157
8-R-11-20-FC	7.16	58.7	12.4	168
4-C-11-20-FC	7.06	62.0	11.1	169
10-R-10-20-FC	6.63	56.5	12.5	160
7-M-20-30-FC	7.32	57.0	13.9	188
12-S-50-60-FC	6.13	45.6	9.38	140
9-B-10-20-FC	5.63	38.9	10.2	148
4-C-21-30-FC	6.43	48.6	9.24	143
10-R-40-45-FC	6.98	44.9	9.89	131
3-B-0-10-FC	6.11	40.8	11.7	156
10-R-31-40-FC	7.17	53.4	10.1	141
14-I-IB	10.9	185	23.5	359
15-R-31-40-FC	11.3	87.5	14.9	252
A-2	5.36	45.3	9.72	142
15-R-IB	10.1	70.7	13.4	226
15-R-11-21-FC	9.41	70.2	13.7	217
4-C-40-50-FC	6.65	44.6	10.5	145
3-B-30-40	8.16	86.7	15.5	229
16-B-21-30-FC	6.85	101	18.6	311
16-B-11-20-FC	7.28	72.4	13.9	235
16-B-31-40-FC	6.96	93.6	16.7	317
15-R-21-30-FC	9.43	73.0	24.4	231
16-B-51-60-FC	6.83	96.6	16.9	310
16-B-0-10-FC	9.45	125	19.8	293
16-B-41-50-FC	7.40	95.6	16.3	297
15-R-0-10-FC	8.31	63.7	14.6	229
13-I-IB	6.71	110	15.6	257
1-M-IB	9.82	99.3	17.0	248
8-R-IB	8.33	324	26.1	265
5-M-IB	10.2	442	44.9	346
10-R-IB	5.99	114	14.7	168

Sample Name	As	Cu	Pb	Zn
16-B-IB	12.6	269	25.0	378
11-S-IB	10.2	314	25.8	319
12-S-0-10-FC	12.5	115	47.4	322
12-S-40-50-FC	6.38	52.9	11.0	168
Waterbottle-TSS	32.8	334	42.0	530
7-M-0-10-FC	8.14	60.3	12.0	217
3-B-20-30	5.13	61.0	10.9	166
12-S-31-40	9.02	71.8	14.8	207
7-M-IB	16.0	567	52.6	540
1-M-IB	8.19	58.5	12.7	219
5-M-20-30	6.42	36.8	11.4	155
6-C-30-41	8.81	81.2	16.3	217
6-C-0-10	8.34	119	24.0	267
11-S-0-10	6.30	61.0	9.81	152
5-M-10-20	6.20	41.5	11.1	171
5-M-30-40	6.47	41.3	11.9	169
11-S-20-31	7.34	45.6	12.1	157
11-S-30-40	6.87	51.7	17.2	169
11-S-10-20	6.85	50.4	9.68	154
5-M-0-10	6.71	44.2	10.9	173
2-C-50-60	6.19	73.7	15.5	198
6-C-40-45	7.06	44.9	9.94	163
2-C-40-50	4.27	69.4	14.4	197
2-C-60-0	5.38	66.9	15.9	191
2-C-30-40	3.46	46.7	12.1	154
6-C-10-20	4.96	43.3	11.7	186
2-C-20-30	3.98	48.5	11.8	157
2-C-0-10	6.36	66.7	17.0	288
6-C-20-30	7.97	96.4	18.9	239
2-C-10-20	9.00	131	24.7	291

*The first two components of the name correspond to location names identified in Figure 1 below. If the sample name only consists of a location, the sample is a bulk sample. If the next component of sample name corresponds to a number then it is from a freeze core and the number corresponds to the sample depth from the surface. Otherwise samples are infiltration bags and designated with an IB.

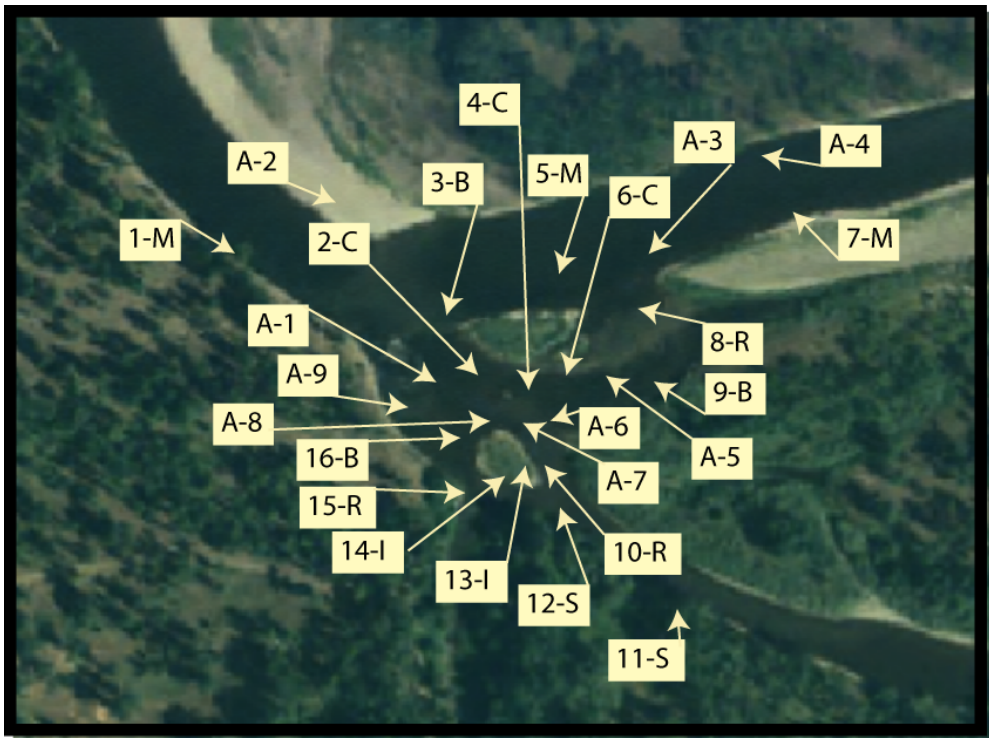

Figure 18-B. Location of samples used in metal analysis.

Blanks

Laboratory blanks ensure lab processing does not add metal content to samples. All of our samples were below detection except for one zinc sample, which was still below instrument accuracy.

Table 12-B. Laboratory blanks below detection level show samples were not contaminated by lab procedures.

Laboratory Blanks				
n=10	**As**	**Cu**	**Pb**	**Zn**
Sample ID	mg/L	mg/L	mg/L	mg/L
LBlank	b.d.	b.d.	b.d.	b.d.
LBlank	b.d.	b.d.	b.d.	b.d.
LBlank	b.d.	b.d.	b.d.	b.d.
LBlank	b.d.	b.d.	b.d.	b.d.
LBlank	b.d.	b.d.	b.d.	b.d.
LBlank	b.d.	b.d.	b.d.	b.d.
LBlank	b.d.	b.d.	b.d.	0.005
LBlank	b.d.	b.d.	b.d.	b.d.
LBlank	b.d.	b.d.	b.d.	b.d.
LBlank	b.d.	b.d.	b.d.	b.d.
LBlank	b.d.	b.d.	b.d.	b.d.

Method blanks are used to assess metal content added by method procedures. Samples for arsenic and lead were below detect. Only one copper sample was detectable and still below instrument detection levels. Zinc concentrations are naturally higher and more variable in nature and are thus more variable within our method blank samples.

Table 13-B. Method blanks show procedures used to prepare sample did not contribute to sample metal concentrations.

Method Blanks				
n=4	As	Cu	Pb	Zn
Sample ID	mg/L	mg/L	mg/L	mg/L
MBLANK	b.d.	0.009	b.d.	0.085
MBLANK	b.d.	b.d.	b.d.	0.024
MBLANK	b.d.	b.d.	b.d.	0.014
MBLANK	b.d.	b.d.	b.d.	0.025

Internal Performance Checks

Internal performance checks are used to maintain calibration of the ICP over the course of sample testing. Continuing calibration verification (CCV) and ICP6, a standard calibration material were used 15 times over the course of sample analysis and were within the measured concentration compared to the nominal concentration were within 10%.

Table 14-B. Continuing calibration verification (CCV) was used to monitor and maintain calibration of instrumentation during sample runs.

CCV				
n=15	As	Cu	Pb	Zn
Sample ID	mg/L	mg/L	mg/L	mg/L
Measured/Nominal Concentration (%)	%	%	%	%
CCV	103	101	99	97
CCV	102	106	98	103
CCV	101	105	96	102
CCV	100	110	96	108
CCV	105	103	97	96
CCV	106	105	96	98
CCV	104	105	95	96
CCV	103	106	95	99
CCV	101	105	93	100
CCV	98	106	92	105
CCV	97	106	91	102
CCV	104	103	100	100
CCV	99	102	96	100
CCV	95	99	93	101
CCV	95	97	93	98

Table 15-B. Statistical summary of CCV. As, Cu and Zn are within the 10% margin of error for mean. One low lead sample skews lowers the mean but the median is still within 10%.

CCV				
n=15	**As**	**Cu**	**Pb**	**Zn**
Measured/Nominal Concentration (%)	%	%	%	%
Mean	91.26	93.95	86.36	90.93
Median	96.68	100.48	92.19	96.77
Range	105.19	104.13	99.42	101.20
Standard Deviation	24.99	25.37	23.48	24.39

Table 16-B. ICP6 is a standard reference material used for calibration.

IPC6				
n=15				
Sample ID	As	Cu	Pb	Zn
Measured/Nominal Concentration (%)	*%*	*%*	*%*	*%*
IPC6	105	99	98	98
IPC6	104	104	99	103
IPC6	106	106	100	105
IPC6	103	107	98	108
IPC6	108	100	100	98
IPC6	110	102	99	98
IPC6	107	101	98	98
IPC6	106	103	97	101
IPC6	105	103	97	103
IPC6	103	105	96	104
IPC6	101	104	95	107
IPC6	108	102	103	104
IPC6	105	101	101	105
IPC6	102	100	98	104
IPC6	98	97	95	103

Table 17-B. Statistical summary of IPC6 concentrations. Mean sample concentration for all metals was within 10%.

IPC6				
n=15	As	Cu	Pb	Zn
Measured/Nominal Concentration (%)	%	%	%	%
Mean	105.0	102.0	98.0	103.0
Median	105.0	102.0	98.0	103.0
Range	12.0	10.0	9.0	10.0
Standard Deviation	3.0	2.6	2.3	3.3

Standard Reference Material

Standard reference materials are used because instruments need to be calibrated to the material of interest. Recovery of NIST2710 demonstrated a low bias, likely due to the age of this standard reference material.

Table 18-B. NIST2710 is a standard reference material used with contaminated soil samples to test the sensitivity of the instrument.

NIST2710	As	Cu	Pb	Zn
n=5	mg/kg	mg/kg	mg/kg	mg/kg
Nominal Conc. (mg/kg)	626	2950	5532	6952
Range (mg/kg)	563	2851	4484	5431
NIST2710	574	3131	4643	6141
NIST2710	571	2916	4291	5364
NIST2710	575	3051	4379	5775
NIST2710	575	2907	4527	5763
NIST2710	575	2907	4527	5763

Table 19-B. Statistical summary of NIST2710 runs. Low bias may be due to the age of the standard reference material.

NIST 2710	As	Cu	Pb	Zn
n=12	mg/kg	mg/kg	mg/kg	mg/kg
Nominal Conc. (mg/kg)	626	2950	5532	6952
Range (mg/kg)	38	130	80	91
mean	571.6	2971.2	4465.1	5694.8
median	574.0	2916.5	4484.5	5763.0
minimum	563.0	2851.1	4291.5	5363.5
maximum	575.0	3130.7	4642.9	6141.1
range	12.0	279.6	351.5	777.5
standard deviation	5.0	115.4	135.4	312.1
mean - nominal conc.	-54.4	21.2	-1066.9	-1257.2
median - nominal concentration	-52.0	-33.5	-1047.5	-1189.0
bias	low bias	low bias	low bias	low bias
precision	2.0	1.6	1.4	0.9
accuracy (%)	8.3	1.1	18.9	17.1

Duplicates

To determine the error in measurement, duplicates are run at different times in the analysis. The concentrations are then compared to evaluate the difference between samples and determine duplicate difference. Lab and method duplicates average measured to nominal concentrations were within 10%.

Table 20-B. Laboratory duplicates are run to assess instrument sensitivity and drift over the course of metal analysis.

Laboratory Duplicates				
n=9	As	Cu	Pb	Zn
Measured/Nominal Concentration	%	%	%	%
LDUP1	2.8	2.2	0.3	1.9
LDUP2	11.0	0.9	4.1	2.3
LDUP3	3.5	3.8	3.4	4.1
LDUP4	4.1	4.0	3.8	1.8
LDUP5	11.0	1.6	1.3	0.7
LDUP6	15.3	0.9	1.5	2.4
LDUP7	1.4	0.8	2.1	3.6
LDUP8	1.1	0.7	0.6	2.2
LDUP9	1.2	2.3	0.7	1.4

Table 21-B. Statistical analysis of laboratory duplicates. Duplicates were fairly accurate, all within 10%.

Laboratory Duplicates				
n=9	As	Cu	Pb	Zn
Measured/Nominal Concentration	%	%	%	%
Mean of Duplicate Difference	5.7	1.9	2.0	2.3
Median of Duplicate Difference	3.5	1.6	1.5	2.2
Range of Duplicate Difference	14.2	3.3	3.8	3.4
Standard Deviation	5.3	1.3	1.5	1.1

Table 22-B. Method duplicates ensure that methods do not dictate sample results.

Method Duplicates				
n=4	As	Cu	Pb	Zn
Measured/Nominal Concentration	%	%	%	%
MDUP1	8.5	10.5	6.1	5.7
MDUP2	6.1	7.0	13.1	3.1
MDUP3	1.2	6.0	7.6	5.8
MDUP3	2.8	1.1	1.9	4.7

Table 23-B. Statistical summary of method duplicates demonstrate that the average duplicate difference was less than 10%.

Method Duplicates				
n=4	**As**	**Cu**	**Pb**	**Zn**
Measured/Nominal Concentration	%	%	%	%
Mean of Duplicate Difference	4.63	6.17	7.18	4.83
Median of Duplicate Difference	4.44	6.52	6.83	5.19
Range of Duplicate Difference	7.29	9.33	11.23	2.72
Standard Deviation	3.27	3.85	4.64	1.26

Spikes

Spikes are used to evaluate the sensitivity of instruments. The lead spikes were lower which is likely due to a weak lead standard. The more robust recovery of other metals indicates that our instruments captured spikes.

Table 24-B. Spikes used to compare the accuracy and sensitivity of metal analysis.

Laboratory Spikes				
n=11	**As**	**Cu**	**Pb**	**Zn**
Measured/Nominal Concentration	%	%	%	%
Lspike	96.2	111.0	90.0	94.4
Lspike	102	117.0	91.0	95.6
Lspike	96.4	117.0	88.0	103.4
Lspike	109.8	119.0	92.0	101.4
Lspike	101.2	110.0	85.0	93.8
Lspike	99.7	111.0	84.0	94.3
Lspike	100.6	115.0	86.0	101.3
Lspike	84.5	101.0	24.0	91.3
Lspike	95.0	103.0	85.0	90.1
Lspike	88.6	101.0	82.0	88.4
Lspike	89.4	100.0	82.0	91.2

Table 25-B. Statistical summary of laboratory spikes. Average measured to nominal concentration for lead is low.

Laboratory Spikes				
n=11	**As**	**Cu**	**Pb**	**Zn**
Measured/Nominal Concentration	%	%	%	%
average	96.6	109.6	80.8	95.0
median	96.4	111.2	85.4	94.3
range	25.3	19.5	68.7	15.0
variance	7.2	7.2	19.3	5.0

Table 26-B. Method spikes test sample processing procedures and sensitivity of these methods to higher metal concentrations.

Method Spikes				
n=8	**As**	**Cu**	**Pb**	**Zn**
Measured/Nominal Concentration	%	%	%	%
Spike Recovery (%)	91	102	84	85
Spike Recovery (%)	98	115	90	97
Spike Recovery (%)	97	113	86	98
Spike Recovery (%)	84	95	78	83
Spike Recovery (%)	94	116	87	103
Spike Recovery (%)	95	105	80	87
Spike Recovery (%)	93	109	81	95
Spike Recovery (%)	98	107	87	94

Table 27-B. Statistical summary of method spikes.

Method Spikes				
n=4	**As**	**Cu**	**Pb**	**Zn**
Measured/Nominal Concentration	**%**	**%**	**%**	**%**
average	93.8	107.8	83.9	92.8
median	94.5	108.1	84.9	94.6
range	14.4	20.2	12.0	20.6
standard deviation	4.8	6.9	4.1	7.2

Metal Analysis Procedure Details

1. Dry sediment sample
2. Separate fine sediment
3. Grind sample in zirconium containers in ball mill for 5 minutes.
4. Weigh and transfer a 0.4 gram (+/- 0.5% or 0.398-0.402 g) to the polypropylene digestion vessel.
5. Add 4 mL of a (1:2) solution of TMG Nitric acid + Milli-Q water and swirl. Cover with reflux cap and heat the sample in the Hot Block at 95°C for 15 minutes without boiling.
6. After the sample is cool add 4 ml conc. TMG Nitric Acid. Then reflux at 95°C for 30 minutes. This step is repeated until no brown fumes appear when TMG Nitric Acid is added.
7. Heat sample with the ribbed watchglass for an additional 1.5 hours.
8. After the sample is completely cool. Cool completely. Add 2 to 5 mL Milli-Q and 0.4 mL of 30% H_{2O2} slowly. After 5 to10 minutes and place the sample back in the Hot Block.
9. Continue to add 0.4 mL of H_{2O2} until the sample remains unchanged in color. Continue heating for a total of 2 hours.
10. After cooling, dilute to 40 mL with Milli-Q, cap and shake the vials, and allow samples to settle overnight. After settling, use the Filtermate for sample filtration.
11. Place sample in ICP vessel.
12. Calibrate ICP
13. Run samples with all associated quality control and assurance as dictated by EPA Method 3050B

C. Hydraulic and Sediment Transport Modeling

My study investigated the spatial and temporal variation of fine sediment infiltration using field data from low flows. Flow over the course of the hydrograph dictates bed mobility, alters flow dynamics and dictates deviations in sediment routing, important controls on FSI. Combining field efforts with modeled shear stress and flow divergence at high flows would aid understanding of process linkages between areas of FSI and quantifiable flow dynamic metrics. Further, modeling would increase the applicability for restoration managers by providing metrics that could be modeled prior to flows of interest, possibly allowing for mitigation efforts. As discussed above, my study evaluates the residence time of fine sediment, substrate reworking, and the role of depositional settings on FSI. Information on spatial variations in flood hydraulics in my field site would provide further insights. For these reasons, I attempted to hydraulically model the field site; this appendix reports progress on that effort. I used a two-dimensional graphical user interface program that can be used to identify bed sediment mobility and flow divergence at different flows (Kinzel et al., 2007).

The International River Interface Cooperative (IRIC) formerly the Multi-Dimensional Surface Water Modeling System (MD_SWMS) designed by the United States Geologic Survey Geomorphology and Sediment Transport is a tool and framework to investigate flow and sediment transport (Nelson, 1996). This graphical user interface hosts a number of models. The Flow and Sediment Transport with Morphological Evolution of Channels (FaSTMECH) is appropriate for our study as a quasi-three dimensional model that incorporates secondary flow components that are associated with curvature and important to modeling the complex field site.

Model assumptions are that flow is incompressible, hydrostatic and quasi-steady state (Nelson et al., 2003). Discharge variations are ignored in the equations of conservation of momentum. Flow is instead approximated by a series of steady state solutions at different discharges. Vertically averaged equations of mass and momentum are solved on a curvilinear orthogonal coordinate system, fitted to the channel around a user-designated centerline (Nelson et al., 2003). There are two stages to the modeling in the FASTMECH model. The first involves using shallow water equations to calculate the vertical structure of streamlines and the cross streamline components for velocity and bed shear stress. Closure for the first stage of modeling is dependent upon shear dictated by user input drag coefficients. The second component of the model calculates secondary flow structures integrating Reynolds shear stress and velocity components around averaged streamline velocities calculated in the first step. Modification of bottom stress due to secondary flows is then incorporated into flow dynamics over time-steps and iterations. The model enables the spatially distributed calculation of velocity and bed shear stress. Using these characteristics, I would identify areas of the bed that have been reworked at different discharges.

Over an approximately 1-km study reach that encompasses the data collection sites described above, topography was characterized using a combination of LiDAR and GPS data. Bathymetry and in-channel features were surveyed with survey-grade Trimble GPS, Leica Total Stations, and deeper bathymetric data was collected with an OHMEX Sonarmite V3 echo sounder. A digital elevation model (DEM) was created using ArcMap to transform data and input x,y,z data (Fig. 1) into IRIC to create a mesh of curvilinear orthogonal grids. Hobo transducers installed at three locations along the study reach provided stage data, both as a downstream boundary condition and for model verification elsewhere in the reach.

Table 28-C. Summary of the data and user inputs for IRIC FaSTMECH model.

Data Inputs	User Inputs
Topography	Centerline
Discharge	Grid Spacing
Stage	Lateral Eddy Viscosity
Water Elevation	Drag Coefficient
	Roughness
	Parameters (Iterations and Relaxation)

A suggestion for model closure is to start and end with a single-thread channel. To do so within my field area, flow must be routed through up to four threads in one cross-section (Fig 2). Surveying the modeled area was labor intensive and survey grade measurements were difficult to obtain in many areas. Additionally, topographic inputs are uncertain in many areas of the river where doing repeat bathymetry was difficult. Legleiter et al. (2007) found modeled depth, velocity and shear stress varied considerably as a function of uncertain topographic inputs. Model closure was achieved for the 2010 peak flow (Fig. 2), but results require further evaluation before being used to draw inferences about FSI. Legleiter et al. (2007) suggest that uncertain topographic inputs altered model findings less at higher discharges.

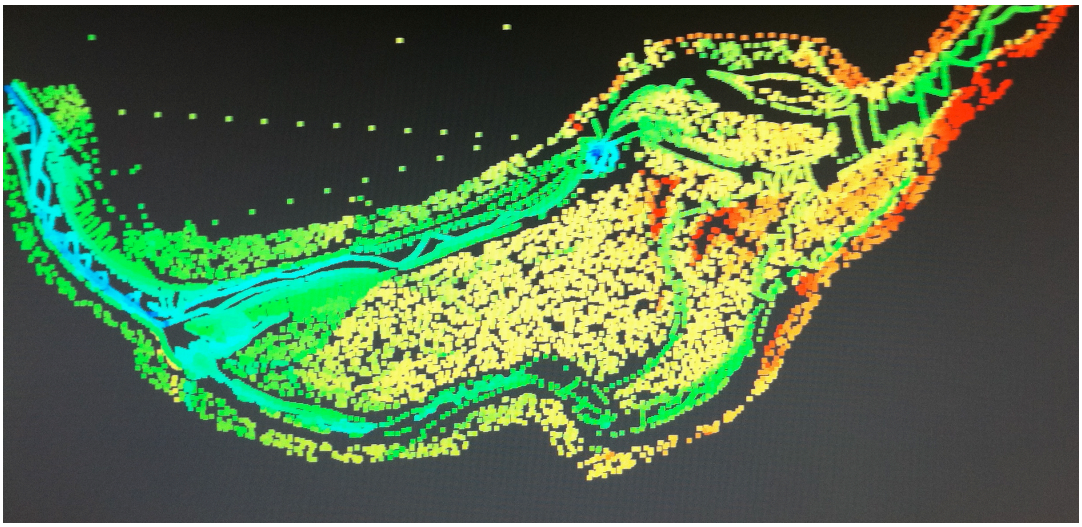

Figure 19-C. Topography input used for peak flow 2010 run, water flows right to left. Note uncertain topography in the first quarter of the modeled reach.

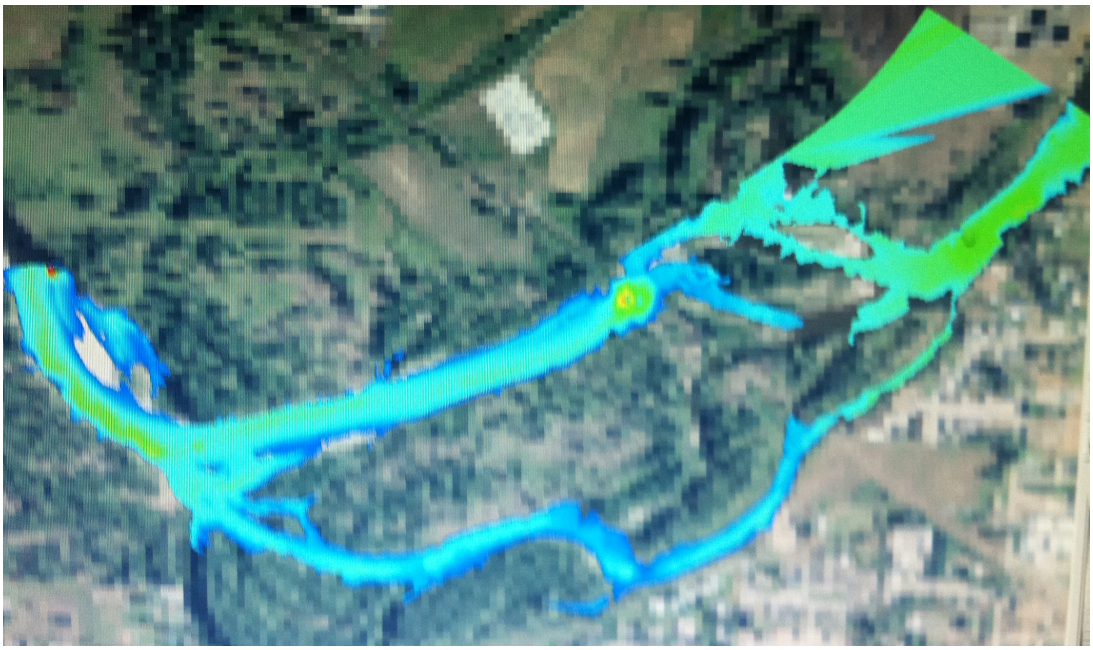

Figure 20-C. Preliminary results for the modeled 2010 peak velocity profile are shown on an aerial photo.

Appendix C References

Kinzel, P.J., Wright, C.W., Nelson, J.M., and Burman, A.R., 2007, Evaluation of an Experimental LiDAR for Surveying a Shallow, Braided, Sand-Bedded River: Journal of Hydraulic Engineering, v. 133, no. 7, p. 838.

Legleiter, C.J., Phelps, T.L., and Wohl, E.E., 2007, Geostatistical analysis of the effects of stage and roughness on reach-scale spatial patterns of velocity and turbulence intensity: Geomorphology, v. 83, no. 3-4, p. 322.

Nelson, J.M., 1996, Predictive techniques for river channel evolution and maintenance: Water, Air, & Soil Pollution, v. 90, no. 1, p. 321.

Nelson, J.M., Bennett, J.P., and Wiele, S.M., 2003, Flow and Sediment-Transport Modeling: Tools in fluvial geomorphology, p. 539.